EVALUATION OF THE STIFFNESS OF INDIVIDUAL LAYERS IN A SPECIALLY DESIGNED PAVEMENT FACILITY FROM SURFACE DEFLECTIONS

By

F. H. Scrivner
Research Engineer

and

W. M. Moore, Ph.D.
Assistant Research Engineer

Research Report Number 32-8

Extension of
AASHO Road Test Results
Research Study Number 2-8-62-32

Sponsored by

The Texas Highway Department
In Cooperation with the
U. S. Department of Commerce, Bureau of Public Road

June, 1966

TEXAS TRANSPORTATION INSTITUTE
Texas A&M University
College Station, Texas

TABLE OF CONTENTS

LIST OF FIGURES

A C K N O W L E D G E M E N T S

The authors appreciate the contribution to this report of Dr. H. O. Hartley, who suggested the composite experiment design given in Table 3; of Professor J. G. Darroch, who wrote the bulk of Section 3 and assisted the authors with other parts of the report; and of Mr. B. H. Atwell, who prepared Appendix A describing measurements of wave velocities in the pavement materials.

The opinions, findings, and conclusions expressed in this publication are those of the authors and not necessarily those of the Bureau of Public Roads.

EVALUATION OF THE STIFFNESS OF INDIVIDUAL LAYERS IN A SPECIALLY DESIGNED PAVEMENT FACILITY FROM SURFACE DEFLECTIONS

(Interim Report)

1. INTRODUCTION

This reporting is being made simultaneously to both the Texas Highway Department and the Highway Research Board, sponsor of a related research project (NCHRP Project 1-6). It describes an assessment of the Lane-Wells Dynaflect as a nondestructive means for estimating the relative stiffness of individual layers in a flexible pavement. It represents an interim report to the Texas Highway Department that will be followed up with a subsequent report after completion of further studies and analyses which are now in progress.

Reference given throughout this report are related to the 1966 model of the Dynaflect. A description and evaluation of the original (1964) model of the Dynaflect was reported to the Texas Highway Department in Research Report 32-4.

The testing employed for the evaluation reported herein was performed on a statistically designed group of experimental pavement sections recently constructed at the Research Annex of Texas A&M University, and financed in part from this research project. The facility is described in Section 3 of the report. Section 4 presents the Dynaflect data, Section 5 is concerned with the development of a mathematical model from elasticity theory, and Section 6 discusses analysis techniques. Section 7 gives the results of the analysis.

Appendix A describes the results of laboratory and field measurements of the velocity of compressional waves through the materials used in the pavement test facility.

Appendix B presents a least-squares regression technique that recognizes the existence of errors of measurement in all variables, in contrast to the classical method which assigns all experimental error to the dependent variable. The technique described in Appendix B was used in the analysis work described in this report.

Conclusions are summarized in the next section.

2. PRINCIPAL CONCLUSIONS

The research reported herein led to the following principal conclusions:

(1) The analysis of Dynaflect data from the Pavement Test Facility resulted in an equation that predicted the deflection basins (measured in each of 27 sections at five points over a distance of four feet) with acceptable accuracy.

(2) The eight coefficients appearing in the equation, each related (by assumption) to the stiffness of one of the eight materials involved in the experiment, appeared to be ordered logically, though one coefficient (that for cement-stabilized crushed limestone), had an illogical sign. According to these coefficients, the stiffness of the materials increased in the order in which the materials are listed below:

1. Undisturbed foundation clay.
2. Same clay, but compacted (in embankment).
3. Sandy clay (in embankment).
4. Sandy gravel (in embankment).
5. Crushed limestone (in base or subbase).
6. Crushed limestone + 2% lime (in base or subbase).
7. Asphaltic concrete (surfacing material).
8. Crushed limestone + 4% cement (in base or subbase).

(3) While the eight material coefficients developed in a single analysis of data from the entire facility appeared to be ordered logically, we did not succeed in showing that logical material coefficients could be found by analysis of data from any single test section, though work toward that end is continuing.

(4) Measurements made on the Pavement Test Facility of seismic wave velocities indicated that "ray theory" seismology was invalid when applied to pavement layers. But velocites determined by the pulse technique are believed to be correct.

(5) The "Multiple Error Regression Technique" used in the analyses has certain advantages over the classical method and should be exploited further. A computer program is available from the writers on request.

3. PAVEMENT TEST FACILITY

Purpose:

The early phases of this research, conducted on existing highways, were dependent upon the available design and construction records for interpretation. It was soon clear that if the equipment used by the measurement team was to include nondestructive testing devices, this equipment would have to be evaluated on road sections whose construction characteristics were known as precisely as possible. The field study demonstrated that normal construction records were not precise enough to characterize the instrument responses observed.

Two nondestructive testing systems were already available for evaluation (the Shell Vibrator System and the Dynaflect), with the likelihood that others would be forthcoming. Therefore, it was decided that the construction of a special pavement test facility was warranted.

As a result of these considerations, a test facility was planned and constructed during the spring and summer of 1965. It is known as the Texas Transportation Institute Pavement Test Facility. Three-fourths of the cost of its construction was paid by this project's funds; the remaining one-fourth was assumed by the Highway Research Board, sponsor of a related research project.

Plan of the Test Facility:

The multiplicity of possible cross-sectional configurations made a well-defined plan imperative. To this end Dr. H. O. Hartley, Director, Institute of Statistics, Texas A&M University, was consulted and the completed facility reflects a selection of configurations based upon sound "design of experiment" principles.

Other possibilities with respect to materials, thicknesses of layers, etc., are acknowledged to exist; however, the possible factors were reduced to six chosen so as to be broadly representative of Texas conditions, as well as being applicable to a much wider area. The six factors included in the plan are listed in Table 1; of these, the first three are quantitative in nature and the remaining three are qualitative. The embankment, base and subbase materials are described in Table 2. Considering the materials in light of the ultimate strengths anticipated, it was believed that they could be quantified, at least as to the approximate order of strengths indicated in Table 2. On this basis all six factors to be included in the plan were assumed to be quantitative and it remained to make a selection of thickness and materials combinations.

Cost of building full scale road sections was estimated to be high; therefore, the number of combinations had to be kept as small as possible. A general knowledge of the nature of the variables suggested that it would be desirable to be able to investigate at least a second degree response surface. These were perhaps the two principal considerations which influenced the choice of design.

The design selected is described as a composite design[1*]. Basically it is made up of two parts: (1) a 1/4 replicate of a 2^6 factorial -- the first 16 treatment combinations (sections) in Table 3, (2) a star consisting of a center point (Section 17) and 12 points on the star (Sections 18 to 29). The six dimensional space we are working in makes it difficult to envision the nature of the design. However, if we consider a three-dimensional space the corresponding design could be described at the 2^3 factorial portion represented by the corners of a cube, the center of the star being the center of mass of the cube, and the star points lying along lines radiating from the center of mass perpendicular to the faces of the cube. Such a design possesses a number of desirable properties, an important one in this case being able to fit a quadratic response surface of the form,

$$Y_u = \beta_o + \sum_{i=1}^{n} \beta_i x_{iu} + \sum_{i=1}^{n} \beta_{ii} x_{iu}^2 + \sum_{i<j}^{n} \beta_{ij} x_{iu} x_{ju} \quad ,$$

(where n represents the number of factors under study), and obtain estimates of all of the regression coefficients, β.

The general plan of the design is shown in the right-hand half of Table 3. Note that any equally spaced set of three levels can be reduced to these $\pm$ 1 and 0 coefficients by the following transformation: $(X_i - \bar{x})/\Delta$, where X_i is the actual level, $\bar{x}$ the mean of the 3 levels (mid-point) and Δ is the increment between levels. The actual design used in constructing the facility is shown in the left-hand half of Table 3, giving the materials and thicknesses to be used in construction.

Some further economy was effected by constructing only 27 sections, rather than the 29 called for by the design. This was possible because Sections 20 and 22 and Sections 21 and 23 were pairwise physically identical; therefore, only Section 20 and 21 were actually constructed. On these two sections it was planned to obtain two independent sets of readings so as to have the set of 29 observations complete for the design. Another decision arrived at in the interests of economy was to construct the facility as three separate units; each unit containing 9 sections where a common embankment material was involved. Thus the final facility was built as displayed in Figures 1 through 4.

Figure 1 is a plan view of the facility, showing the arrangement of the 27 12' x 40' test sections, together with five additional sections included in the turn-around at one end of the project.

Figure 2 is a typical cross-section of the main facility. Figure 3 depicts construction scenes, and Figure 4 is a view of the completed facility.

---

*Superscript numbers refer to references listed in the Biblography.

Special Sections:

The turn-around sections constitute a small experiment in which the single variable was base material type, as indicated in Table 4. Neither a subbase nor an embankment was constructed in these sections, and all were surfaced with a two-course surface treatment approximately 3/4 inch thick. The base in all sections was six inches thick, and the subgrade material was the natural clay, of which only the top 6-to 8-inch layer was compacted.

TABLE 1

List of Variables

Variable	Levels		
	Low (-1)	Medium (0)	High (+1)
Surface Thickness	1"	3"	5"
Base Thickness	4"	8"	12"
Subbase Thickness	4"	8"	12"
Base Material Type	4	5	6
Subbase Material Type	4	5	6
Subgrade Material Type	1	2	3

TABLE 2

Materials Used in Embankment, Base and Subbase

Material* Type	Description	Where Used	AASHO Class.	Unified Soil Class.	Texas Triaxial Class.	Compressive Strength** psi
1	Plastic Clay	Embankment	A-7-6(20)	CH	5.0	22
2	Sandy Clay	Embankment	A-2-6(1)	SC	4.0	40
3	Sandy Gravel	Embankment	A-1-6	SW	3.6	43
4	Cr. Limestone	Base & Subb	A-1-a	GW-GM	1.7	165
5	Cr. Limestone + 2% Lime	Base & Subb	A-1-a	GW-GM		430
6	Cr. Limestone + 4% Cement	Base & Subb	A-1-a	GW-GM		2270

* The six materials are numbered in the assumed order of increasing strength.

** By Texas triaxial procedure, at a lateral pressure of 5 psi.

NOTE: The foundation material (Material Type 0) and the asphaltic concrete surfacing material (Material Type 7) were not variables in the experiment.

TABLE 3

Experiment Design

Sec. No.	Actual Design: Layer Thick. (In.) Sur.	Base	Subb.	Matl. Type* Base	Subb.	Subg.	Theoretical Design: Thick Level Sur.	Base	Subb.	Strength Level Base	Subb.	Subg.
1	5	4	4	6	4	1	+1	-1	-1	+1	-1	+1
2	1	12	4	6	4	1	-1	+1	-1	+1	-1	+1
3	1	4	12	6	4	1	-1	-1	+1	+1	-1	+1
4	5	12	12	6	4	1	+1	+1	+1	+1	-1	+1
5	5	4	4	4	6	1	+1	-1	-1	-1	+1	+1
6	1	12	4	4	6	1	-1	+1	-1	-1	+1	+1
7	1	4	12	4	6	1	-1	-1	+1	-1	+1	+1
8	5	12	12	4	6	1	+1	+1	+1	-1	+1	+1
9	5	4	4	4	4	3	+1	-1	-1	-1	-1	+1
10	1	12	4	4	4	3	-1	+1	-1	-1	-1	+1
11	1	4	12	4	4	3	-1	-1	+1	-1	-1	+1
12	5	12	12	4	4	3	+1	+1	+1	-1	-1	+1
13	5	4	4	6	6	3	+1	-1	-1	+1	+1	+1
14	1	12	4	6	6	3	-1	+1	-1	+1	+1	+1
15	1	4	12	6	6	3	-1	-1	+1	+1	+1	+1
16	5	12	12	6	6	3	+1	+1	+1	+1	+1	+1
17	3	8	8	5	5	2	0	0	0	0	0	0
18	1	8	8	5	5	2	-1	0	0	0	0	0
19	5	8	8	5	5	2	+1	0	0	0	0	0
20	3	4	8	5	5	2	0	-1	0	0	0	0
21	3	12	8	5	5	2	0	+1	0	0	0	0
**22	3	8	4	5	5	2	0	0	-1	0	0	0
**23	3	8	12	5	5	2	0	0	+1	0	0	0
24	3	8	8	4	5	2	0	0	0	-1	0	0
25	3	8	8	6	5	2	0	0	0	+1	0	0
26	3	8	8	5	4	2	0	0	0	0	-1	0
27	3	8	8	5	6	2	0	0	0	0	+1	0
28	3	8	8	5	5	1	0	0	0	0	0	-1
29	3	8	8	5	5	3	0	0	0	0	0	+1

*See Table 2 for description of materials.
**Duplicate section, not constructed.

TABLE 4

Base Materials Used In
Turn-around Sections

Section Number	Base Material Type*
30	2
31	6
32	4
33	5
34	3

*See Table 2 for Description of Materials.

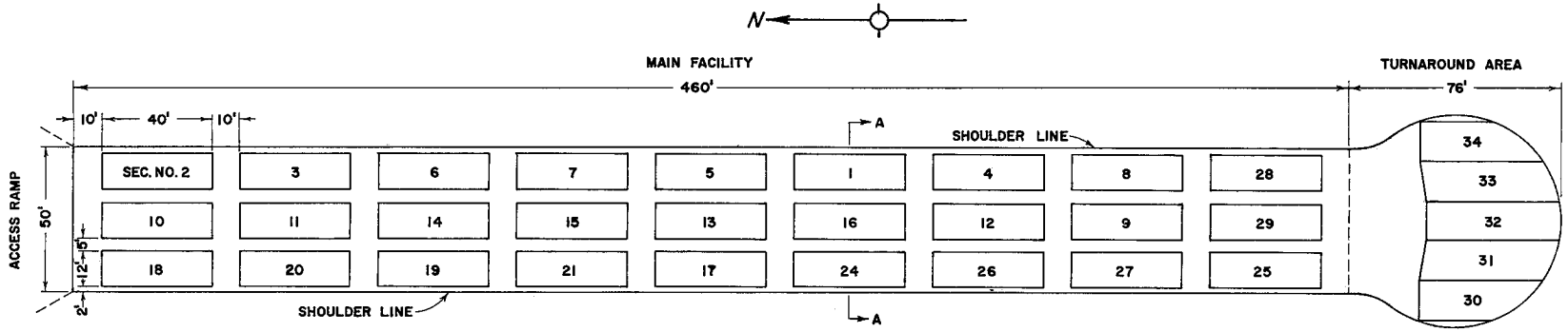

Figure 1: Plan view of pavement test facility

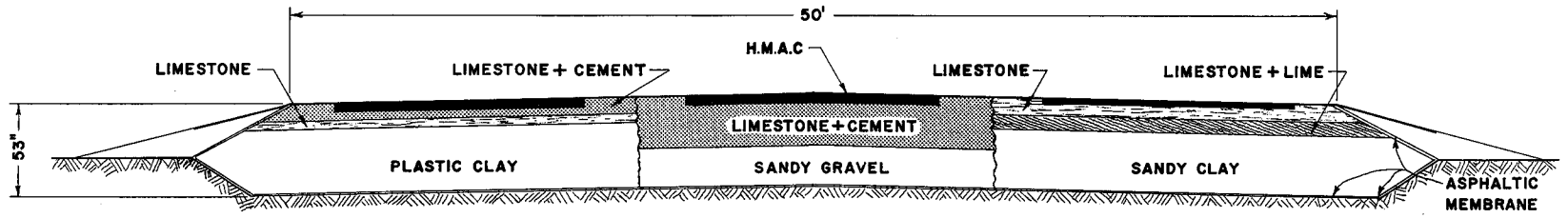

Figure 2: Cross-section of pavement test facility (Section A-A of Figure 1)

Figure 3: Test facility construction. Spreading crushed limestone (upper) and mixing water and lime with Rex Chain-Belt Pulvimixer (lower)

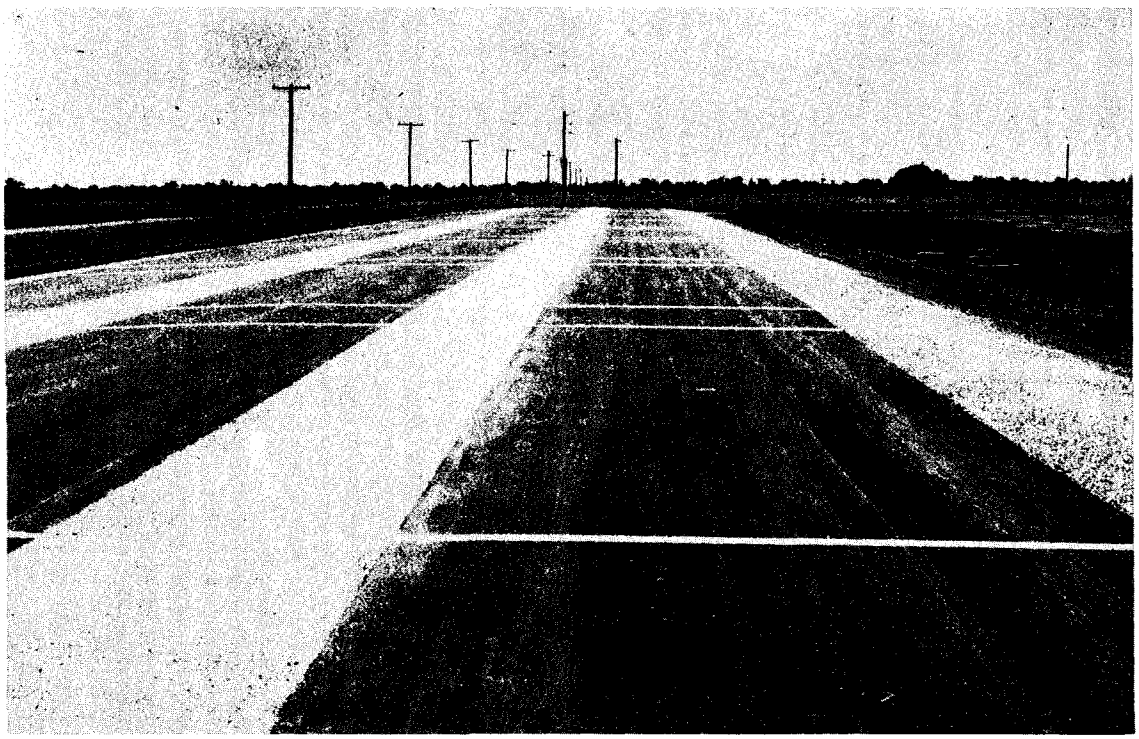

Figure 4: View of completed facility

4. DYNAFLECT DATA FOR ANALYSIS

Figure 5, a schematic drawing of a block cut out of the pavement test facility, shows the relative positions of the loaded points, as well as the points where deflections were measured by the Dynaflect system. The deflection or geophone points, numbered 1 through 5 in the sketch, will be identified throughout this report by those numbers.

Though more than usual care was taken in the construction of the test facility to insure as uniform results as possible, tests with the Dynaflect indicated some variation in the deflections measured at different locations on a test section. For this reason, data for the analysis reported herein were taken in each section at six of the eight locations indicated in Figure 6, and were averaged prior to the analysis.

The data were gathered on March 9, 10, 11 and 14, 1966, during the hours from 8 a.m. to 5 p.m. Figure 7 is a plot of air temperatures recorded at Easterwood Airport (located 7 miles from the test facility) during the test period. The average hourly temperature between 8 a.m. and 5 p.m., on the four days the testing was carried out, was 65.1°F.

Though temperature is known to affect deflection because of its influence on the asphaltic concrete surfacing, the order in which the sections were tested was such as to achieve a randomization of the temperature variable. Thus the effect of temperature should not bias the analysis of the deflection data.

Table 5 lists the averaged Dynaflect data as well as section design data used in the analysis. The symbols appearing in this table are the same as the symbols used in the mathematical model described in the next section of the report.

In the first column of Table 5 is given the test section identification number. This column is the same as column 1 of Table 1, except that in Table 5, Sections 22 and 23 do not appear, since (as mentioned earlier) these sections were not constructed.

The second column of Table 5 gives a section index number, k (k = 1, 2, ..., 27).

The third column lists a material index number, j, identifying the materials used in constructing each section (j =1, 2, ..., 7). These numbers (with the exception of the number, 7) are also given in the first column of Table 2, where six of the seven materials used in the test facility are described. The number, 7, was assigned to the asphaltic concrete surfacing material, and (as indicated at the bottom of Table 5), the number 0 was assigned to the foundation material below the embankments.

The fourth and fifth columns of Table 5 show the depths below the surface, H_{1jk} and H_{2jk}, of the top and bottom of the layer composed of material j in section k. (Note that the order in which the layers were constructed in a section is not necessarily the order indicated by the index, j. For example, see Section 5 in Table 5).

The remaining columns in Table 5 give the deflection, W_{ik}, registered by the ith geophone (i = 1, 2, ..., 5) on the kth section (k = 1, 2, ..., 27).

Table 5 presents quantitatively all the information available for analysis with the exception of a set of dimensions describing the location of each of the five geophones with respect to the loads applied to the pavement by the Dynaflect. Since the arrangement of the geophones and loads was the same on all test sections, and because of the symmetry of this arrangement (see Figure 7), the dimension selected to describe the location of the ith geophone was the distance, r_i, from that geophone to either of the two loads. Table 6 gives the value of r_i^2 (i = 1, 2, ..., 5).

The primary purpose of the analysis of the data in Tables 5 and 6 was to provide a basis for accepting or rejecting the following hypotheses:

(a) Given the values of W_{ik}, H_{1jk}, H_{2jk} and r_i tabulated in Tables 5 and 6, it is possible to estimate, with reasonable accuracy, the relative stiffness of the eight materials occurring in the 27 test sections.

(b) Given data limited to a single test section, it is possible to estimate with reasonable accuracy the relative stiffness of the four or five materials occurring in that section.

Before performing the analysis it was necessary to construct a trial mathematical model relating the variables named above and containing coefficients assumed to be associated with the stiffness property sought from the analysis. The next section of the report is concerned with the construction of such a model.

TABLE 5

DYNAFLECT DATA TAKEN MARCH 9 - 14, 1966
AND
SECTION DESIGN DATA FOR PAVEMENT TEST FACILITY

(Each tabulated deflection is the average of six measurements.)

Sec.No.	Sec. Index k	Mat'l Index j	Depth to Top and Bottom of Layer (Inches) H_{1jk}	H_{2jk}	Deflection, W_{ik} (milli-inches) i=1	i=2	i=3	i=4	i=5
1	1	1	13	53	1.92	1.49	1.01	.60	.36
		4	9	13					
		6	5	9					
		7	0	5					
2	2	1	17	53	.52	.47	.41	.34	.29
		4	13	17					
		6	1	13					
		7	0	1					
3	3	1	17	53	1.05	.86	.58	.39	.29
		4	5	17					
		6	1	5					
		7	0	1					
4	4	1	29	53	.37	.35	.32	.28	.25
		4	17	29					
		6	5	17					
		7	0	5					
5	5	1	13	53	1.26	.95	.61	.40	.28
		4	5	9					
		6	9	13					
		7	0	5					
6	6	1	17	53	1.16	.96	.72	.49	.35
		4	1	13					
		6	13	17					
		7	0	1					
7	7	1	17	53	.74	.65	.53	.42	.33
		4	1	5					
		6	5	17					
		7	0	1					
8	8	1	29	53	.62	.43	.33	.28	.24
		4	5	17					
		6	17	29					
		7	0	5					

TABLE 5 (CONTINUED)

Sec.No.	Sec. Index k	Mat'l Index j	Depth to Top and Bottom of Layer (Inches) H_{1jk}	H_{2jk}	Deflection, W_{ik} (milli-inches) i=1	i=2	i=3	i=4	i=5
9	9	3	13	53	.75	.55	.38	.27	.21
		4	5	13					
		7	0	5					
10	10	3	17	53	.63	.50	.40	.32	.26
		4	1	17					
		7	0	1					
11	11	3	17	53	.63	.48	.37	.28	.23
		4	1	17					
		7	0	1					
12	12	3	29	53	.64	.45	.32	.25	.20
		4	5	29					
		7	0	5					
13	13	3	13	53	.47	.43	.36	.28	.22
		6	5	13					
		7	0	5					
14	14	3	17	53	.40	.37	.33	.27	.23
		6	1	17					
		7	0	1					
15	15	3	17	53	.41	.36	.32	.27	.22
		6	1	17					
		7	0	1					
16	16	3	29	53	.29	.26	.25	.21	.19
		6	5	29					
		7	0	5					
17	17	2	19	53	.72	.59	.44	.33	.26
		5	3	19					
		7	0	3					
18	18	2	17	53	.84	.66	.48	.36	.28
		5	1	17					
		7	0	1					
19	19	2	21	53	.76	.64	.48	.36	.28
		5	5	21					
		7	0	5					

TABLE 5 (CONTINUED)

Sec.No.	Sec. Index k	Mat'l Index j	Depth to Top and Bottom of Layer (Inches) H_{1jk}	H_{2jk}	Deflection, W_{ik} (milli-inches) i=1	i=2	i=3	i=4	i=5
20	20	2	15	53	.73	.61	.47	.35	.27
		5	3	15					
		7	0	3					
21	21	2	23	53	.62	.53	.42	.33	.27
		5	3	23					
		7	0	3					
24	22	2	19	53	.91	.67	.46	.34	.26
		4	3	11					
		5	11	19					
		7	0	3					
25	23	2	19	53	.47	.43	.38	.32	.26
		5	11	19					
		6	3	11					
		7	0	3					
26	24	2	19	53	.69	.58	.45	.34	.26
		4	11	19					
		5	3	11					
		7	0	3					
27	25	2	19	53	.80	.67	.51	.38	.30
		5	3	11					
		6	11	19					
		7	0	3					
28	26	1	19	53	1.05	.86	.62	.43	.30
		5	3	19					
		7	0	3					
29	27	3	19	53	.51	.43	.35	.28	.22
		5	3	19					
		7	0	3					

Note: The material index, j, for the foundation on which the embankments were constructed, is j = 0. For every test section, $H_{10k} = 53$ and $H_{20k} = \infty$.

TABLE 6

Geophone Index, i	r_i^2
1	100
2	244
3	676
4	1396
5	2404

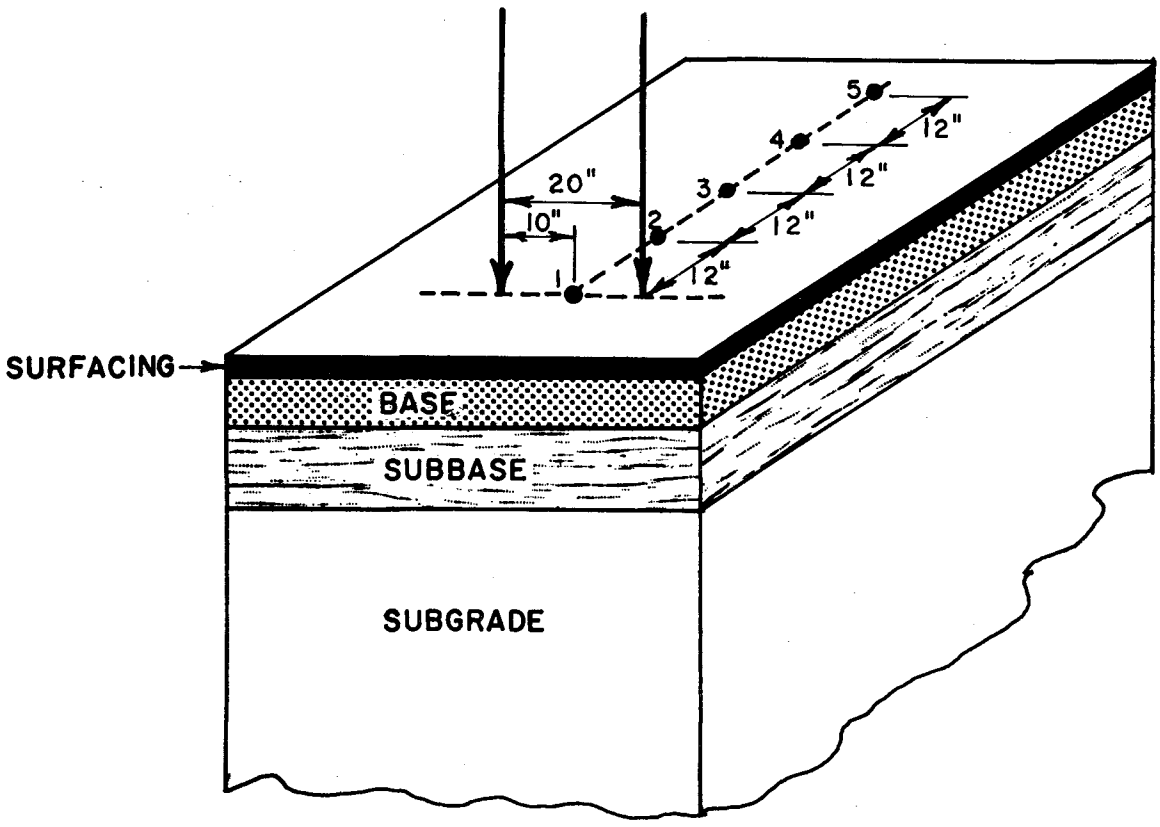

Figure 5: Position of Dynaflect sensors and load wheels. The vertical arrows represent the load wheels and the points numbered 1 through 5 represent the position where sensors 1 through 5 pick up the motion of the pavement surface

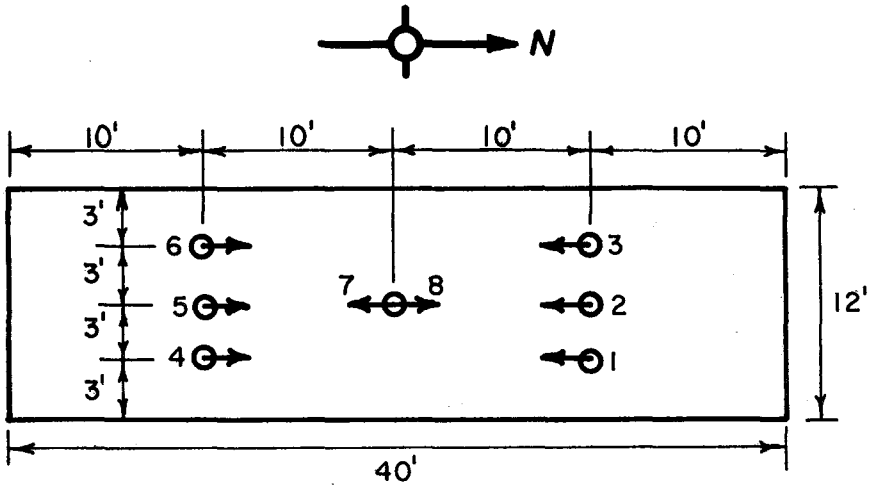

Figure 6: Location of test points in a test section. Dynaflect data was taken with sensor No. 1 (See Figure 5) located at one of the test points and the other sensors located in the direction of the arrow

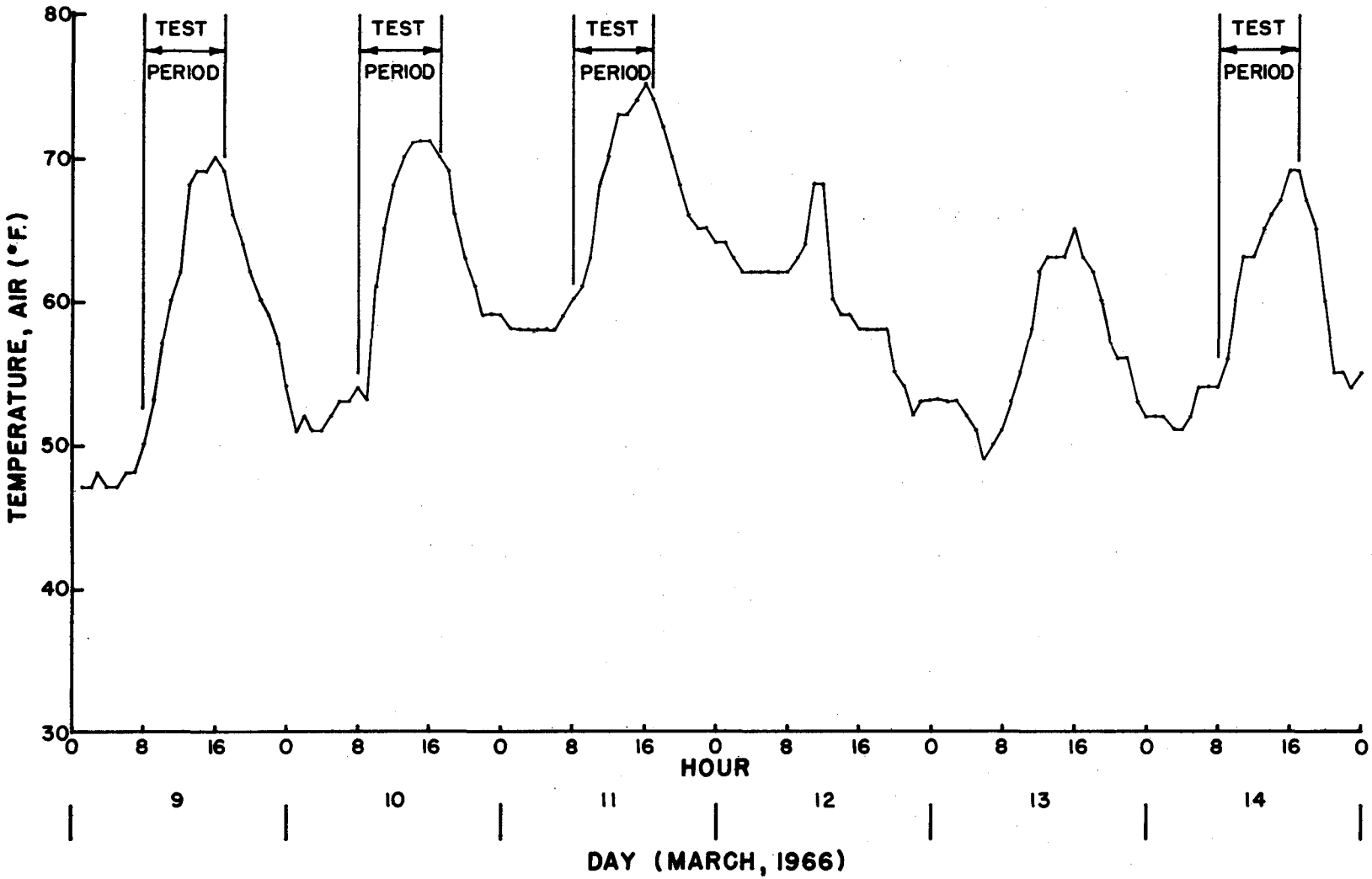

Figure 7: Air temperature during test periods

5. TRIAL MODEL FOR USE IN ANALYSIS

The deflection at any point in an elastic, layered system can be estimated from elasticity theory, if one is given the thickness, the Young's modulus, and the Poisson's ratio of each layer[2,3]. In the present instance, however, it was required to estimate the Young's modulus of each layer, given the thickness of each, and the deflection measured at five points on the surface. The use of rigorous theory for this purpose appeared to be a task of impossible complexity. It was decided, therefore, to use elasticity theory in part, but to take certain liberties with the theory in order to obtain a useable mathematical model. It was reasoned that if such a model "worked" -- that is, reproduced the measured data with acceptable accuracy and yielded logical values of the coefficients -- then its use would be justified in spite of the approximations involved in its derivation.

The derivation of a trial model follows:

We begin by considering the deflection produced by a point load. In Figure 8, Q_1 is a point with cylindrical coordinates, $r = r_i$ and $z = H_2$, located in the interior of the semi-infinite, homogenous, elastic body bounded by the horizontal plane, $z \geq 0$. A second point, Q_2, located directly beneath Q_1, has the coordinates, $r = r_i$ and $z = H_2$. A point load, P acts perpendicular to the boundary plane at the origin of coordinates, 0.

We define W_1 as the vertical displacement (positive in a downward direction) of point Q_1, and W_2 as the vertical displacement of point Q_2.

We also define Δw by the equation,

$$\Delta w = W_1 - W_2 \quad , \qquad (1)$$

where Δw is the change in length of the line Q_1Q_2 caused by application of the point load, P. Δw is positive if the line Q_1Q_2 is shortened.

Then, according to elasticity theory[4], it can be shown that Δw is given by the following:

$$\Delta w = \frac{P}{2\pi}\,\frac{1+\mu}{E}\left[\frac{2(1-\mu)r_i^2 + (3-2\mu)H_1^2}{(r_i^2 + H_1^2)^{3/2}} - \frac{2(1-\mu)r_i^2 + (3-2\mu)H_2^2}{(r_i^2 + H_2^2)^{3/2}}\right] \qquad (2)$$

Consider now a layer of material bounded by the horizontal planes, $z = H_1$ and $z = H_2$, indicated in Figure 8 by the dashed lines, A_1B_1 and A_2B_2. The vertical line Q_1Q_2 is the original thickness of the layer, and Δw is the change in thickness at the horizontal distance, r_i, from the point of application of the load.

We suppose the half-space in Figure 8 to be made up of q layers such as the one just described, each layer being of finite thickness except the lowest -- or foundation -- layer which extends downward to infinity.

Contrary to our previous assumption of homogenity, and departing from rigorous theory, we now suppose that the Young's modulus of the material composing any layer, while constant within the layer, differs from that of every other material in the system. We assign a number, represented by the symbol, j, to each such material, and use j as a subscript on symbols representing quantities associated with the jth material. (j = 1, 2, ..., q).

Thus, E_j is Young's modulus for the jth material while H_{1j} is the depth of the upper boundary and H_{2j} the depth of the lower boundary of that material. Δw_{ij} is the change in thickness of the jth material, occurring at the horizontal distance r_i from the point of load application.

While Young's modulus, E, is assumed to vary from one material to the next, Poisson's ratio, μ, is assumed to be the same for all materials.

We now define W_i as the vertical displacement of a point on the pavement surface at the distance r_i from the point of load application. Then W_i is the sum of the Δw_{ij}; that is

$$W_i = \sum_{j=1}^{q} \Delta w_{ij} \quad , \tag{3}$$

where (according to Equation 2 and the definitions of the subscripts i and j) Δw_{ij} is given by

$$\Delta w_{ij} = \frac{P}{2\pi} \frac{1+\mu}{E_j} \left[\frac{2(1-\mu) r_i^2 + (3-2\mu) H_{1j}^2}{(r_i^2 + H_{1j}^2)^{3/2}} - \frac{2(1-\mu) r_i^2 + (3-2\mu) H_{1j}^2}{(r_i^2 + H_{2j}^2)^{3/2}} \right] \tag{4}$$

We note from Figure 3 that the distance, r_i, measured from either of the two Dynaflect loads, is the same. Thus Equation 4 applies to either load, and the effect of both loads is obtained simply by multiplying the right side of Equation 4 by 2.

However, to use Equation 3 and 4 as the basis for a model to be used in a regression analysis of Dynaflect data collected on the 27 sections comprising the test facility, it is necessary to introduce a third subscript, k, designating the test section (k = 1, 2, ..., 27).

By attaching the subscript k to the appropriate symbols, we form the trial regression model as follows:

$$W_{ik} = \sum_{j=0}^{7} A_j X_{ijk} \quad , \tag{5}$$

where $i = 1, \ldots, 5.$ (i = geophone index).

$j = 0, \ldots, 7.$ (j = material index).

$k = 1, \ldots, 27.$ (k = section index).

W_{ik} = deflection measured by geophone i on section k.

$$A_j = \frac{P}{\pi} \frac{1-\mu^2}{E_j} = \text{constants determined by regression analysis.} \tag{6}$$

P = load on one load wheel of Dynaflect.

μ = Poisson's ratio, assumed to be the same for all materials.

E_j = Young's modulus of material j.

$$X_{ijk} = \frac{r_i^2 + BH_{1jk}^2}{(r_i^2 + H_{1jk}^2)^{3/2}} - \frac{r_i^2 + BH_{2jk}^2}{(r_i^2 + H_{2jk}^2)^{3/2}} \quad . \tag{7}$$

$$B = \frac{3-2\mu}{2(1-\mu)} \tag{8}$$

r_i = Distance from either point of load application to geophone i.

H_{1jk} = Depth of upper boundary of material j in section k.

H_{2jk} = Depth of lower boundary of material j in section k.

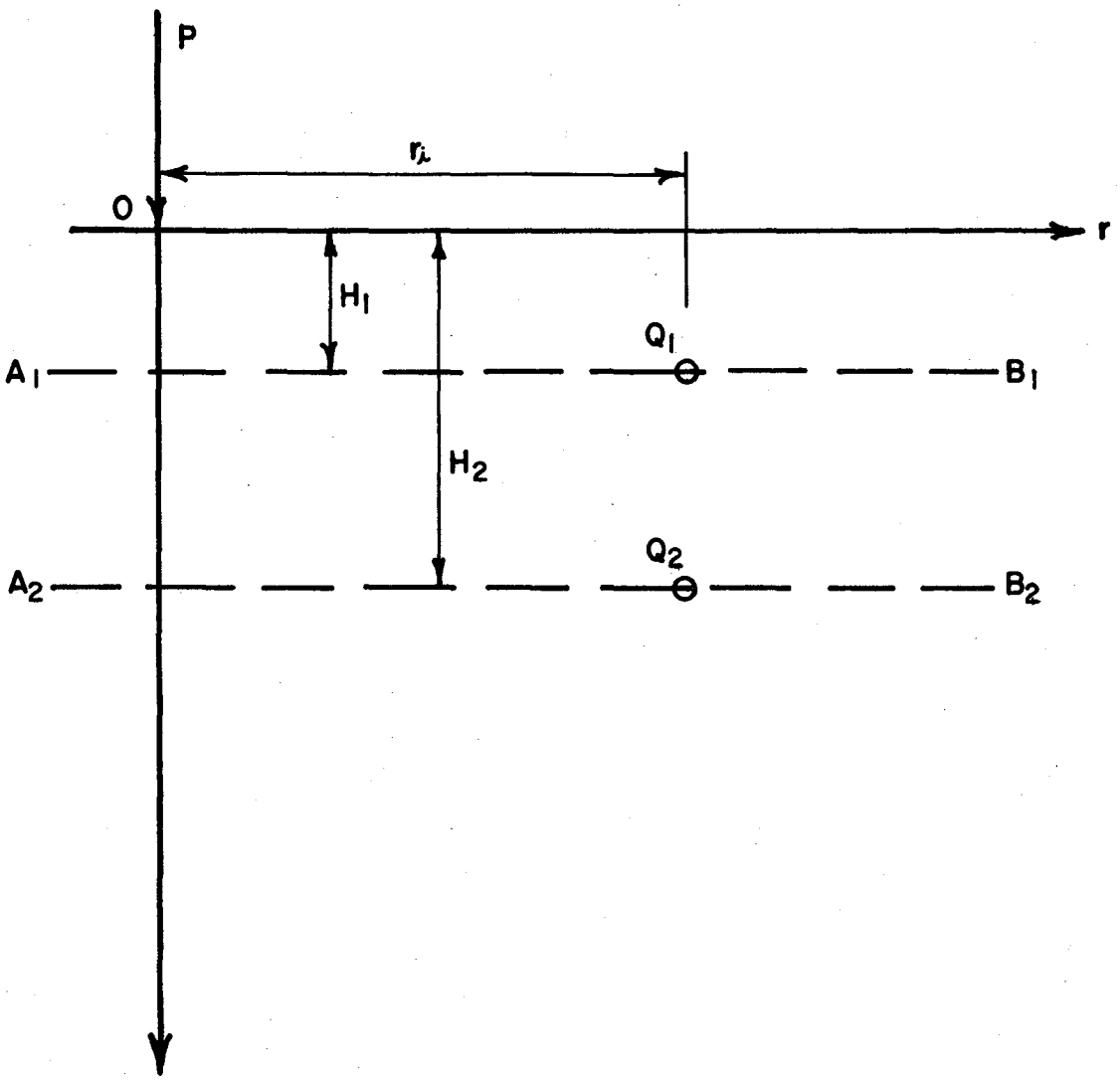

Figure 8: Vertical point load, P, acting on the boundary plane, $z \geq 0$, of a semi-infinite, elastic body

6. TECHNIQUE USED FOR DETERMINING THE COEFFICIENTS, A_j

The coefficients, A_j, in Equation 5 can be determined by classical regression methods for any assigned value for the constant B. By assigning several values to B, and performing an analysis for each, the particular value of B resulting in the least error in predicting the deflection data can be found. The corresponding values of the coefficients, A_j, then would be regarded as the best estimates of their true values that could be made from the data.

The above procedures were used in the investigation of the trial model with one exception: a regression technique different from the classical method was employed, for the reasons advanced below.

In the classical method of fitting a linear model to data collected in an experiment involving several variables, it is assumed that the values of all but one - the dependent or response variable - are known precisely. Frequently, however, there are errors of measurement in all the variables. In such cases (and the present instance is an example) the classical method yields a biased estimate of the regression coefficients. Since the objective of this experiment was to obtain unbiased estimates of the coefficients, A_j, it was apparent that the probability of error in the variables, X_{ijk}, should not be ignored.

The "Multiple Error Regression Technique" described in Appendix B makes allowances for measurement errors in all the variables entering into an analysis. Therefore, this technique, rather than the classical method, was used in the analyses reported herein.

The multiple error method requires that the user estimate the ratio of the <u>quality</u> of each controlled variable, to the quality of the response variable, the quality of the variable being defined as the ratio of its variance to the variance of the errors made in measuring it. For the analyses reported here, the quality of each variable, X_{ijk}, was taken to be ten times the quality of the response variable, W_{ik}. (In contrast to this 10 to 1 ratio, use of the classical method would require that the ratio be infinite.)

For further details regarding the quality of variables, as well as other features of the multiple error regression technique, the reader is referred to Appendix B, and in particular to the example given at the end of the appendix.

7. RESULTS OF ANALYSIS

From the data listed in Tables 5 and 6, and by use of the procedures outlined in Article 5, the coefficients A_j of Equation 5 were determined for a wide range of values of the constant, B. Within the logical range of this constant, $1.5 \leq B \leq 2.0$, (corresponding to the full range from zero to one-half of Poisson's ratio) the prediction errors were relatively large. For certain values of B well outside its logical range, the prediction errors were relatively small but the predicted shape of the deflection basins for several of the 27 test sections differed radically from the shapes observed. These results were not considered acceptable. Consequently, the model was altered in several respects so that it would satisfy certain conditions calculated to insure better results. The conditions, three in number, are stated below.

With the coefficient, A_j, positive and fixed in value, the compression, $\Delta W_{ijk} = A_j X_{ijk}$, of the layer composed of material j, must satisfy the following inequalities:

$$\frac{\partial \Delta W_{ijk}}{\partial r_i} < 0 \qquad \text{(Condition 1)}$$

$$\frac{\partial \Delta W_{ijk}}{\partial H_{1jk}} < 0 \qquad \text{(Condition 2)}$$

$$\frac{\partial \Delta W_{ijk}}{\partial H_{2jk}} > 0 \qquad \text{(Condition 3)}$$

Condition 1 insures that the surface deflection decreases as r_i increases.

Condition 2 insures that the compression of any layer decreases if it is made thinner - or increases if it is made thicker - by lowering or raising its upper boundary.

Condition 3 insures that the compression of any layer increases if it is made thicker - or decreases if it is made thinner - by lowering or raising its lower boundary.

The first trial model (Equation 5) met these conditions only within a limited range of the variables r_i, H_1 and H_2.

The net effect of imposing these three restrictions upon the model was to insure that the deflection basin predicted by the model would always be normal in shape, provided that the values of the coefficients, A_j, determined from the data, were positive and logically ordered. The second trial model, which conforms to the conditions listed above, is given below:

$$W_{ik} = \sum_{j=0}^{7} A_j X_{ijk} \quad , \qquad (9)$$

where,

$$X_{1jk} = \frac{1}{(cr_i^a + H_{1jk}^a)^b} - \frac{1}{(cr_i^a + H_{2jk}^a)^b} \quad . \qquad (10)$$

In these expressions, a, b and c are constants, and the coefficients, A_j, are assumed to be inversely related to the resistance of the corresponding materials to compression under load; that is, a relatively small value of A would be associated with a relatively stiff material.

From a series of regression analyses, each performed with a different set of values assigned to a, b and c, the particular set of three constants and eight coefficients that resulted in the least prediction error was found. This set is given in Table 7.

The prediction error (the root-mean-square residual shown in Table 7) was relatively small, being 14.3% of the mean value of the observed deflections.

As may be seen in Table 7, one coefficient, that for cement-stabilized crushed limestone, was illogical in sign. The reason for this is not clear, but it may stem from the fact that this material was apparently much more rigid than the others, and perhaps contributed so little to the surface deflections that its contribution, represented by the term $A_6 X_{i6k}$ in Equation 9, could not be sensed by the geophones. Under these conditions, normal experimental error in the data could have caused the reversal in sign.

For comparison with the coefficients, two independent measures of material properties, compressive strength and pulse velocity, are given in Table 7 for the six materials appearing as variables in the experiment design. The compressive strengths are determined from triaxial tests performed at a constant lateral pressure of 5 psi in accordance with standard Texas Highway Department procedures.[5] The pulse velocities were measured on the compacted materials in place during construction, by the method described in Appendix A, and were necessarily determined before the stabilized materials (Types 5 and 6 in Table 7) had completely cured.

If one interprets the negative coefficient for Material 6 as meaning that the coefficient is very small (being algebraically smaller than any of the others), then it is apparent from Table 7 that the coefficients A_1 through A_6 occur in the inverse order of compressive strength and pulse velocity, as might be expected. This is taken as evidence that (1) the model does represent the physical phenomena with some degree of accuracy, and (2) the response of the dynaflect does depend upon the stiffness and thickness of the structural components of the pavement.

That a functional relationship exists between the coefficients, A_j ($j = 1$ through 5) and the corresponding compressive strengths, S_j given in Table 7, is suggested by Figure 9, where log A has been plotted against log S.

The straight line shown on the graph was fitted by the multiple error method with the quality of the two variables assumed to be equal. The correlation coefficient was 0.98.

A similar correlation exists between log A and the pulse velocity, V, as indicated in Figure 10. As in the preceding figure, the straight line shown in Figure 10 was fitted by the multiple error method with the quality of the two variables assumed to be the same. The correlation coefficient was 0.99.

The equations for the lines shown in Figures 10 and 11 are given below:

$$\log A = 0.8547 - 1.3554 \log S \quad (11)$$

$$\log A = 0.2472 - 5.2596\ V \times 10^{-4} \quad (12)$$

In the derivation of these equations from the data in Table 7, data for Material 6 could not be used, since the sign of A_6 was negative. Each equation, however, may be used to predict a value of A_6 that will be consistent with the data provided by Materials 1 through 5 that were used in deriving the equations. The value predicted from the compressive strength of Material 6 is 2.0×10^{-4}, while the value predicted from its pulse velocity is 2.5×10^{-4}. Both values are smaller than the coefficient for asphaltic concrete (5.7×10^{-4}), indicating that the latter material was not as stiff as the cement stabilized crushed limestone. This conclusion is supported by the opinion of members of the project staff who are familiar with the Pavement Test Facility and the materials used in its construction.

Predictions from Equation 9, using the coefficients and constants given in Table 7, are shown as curved lines in Figures 11A through 11D for each section, while the observed data are plotted as circled points. The influence of the illogical sign of A_6 is clearly evident in the graphs for Sections 2, 3, 14, 15 and 16.

Also evident from the graph for Section 1 (Figure 11A) is a large discrepancy between the observed data and the predicted deflection basin. The deflections observed on this section are known to be inconsistent with the design of the section, though an investigation into the possible causes of the excessive deflections has not yet been completed. A similar inconsistency, though less pronounced, was discovered in the data from Section 3. Because the data from Sections 1 and 3 had a markedly adverse effect on the trial analyses, deflections from those two sections were not used in the analysis summarized in Table 6. Elimination of these data reduced the total number of observations available for analysis from 135 to 125.

In order to obtain from the coefficients given in Table 7 a prediction equation with logical values for all eight coefficients, a new set of coefficients, A_j', was found by the following two-step procedure:

(1) A factor, F, was computed from the following equation:

$$F = \frac{\overline{W}}{\sum_{j=0}^{7} A_j \overline{X}_j} \tag{13}$$

where $\overline{W}$ = the mean of W_{ik} given in Table 7,
A_j = coefficients given in Table 7, except that A_6 is taken as 2.25×10^{-4}, which is the average of the values (2.0×10^{-4} and 2.5×10^{-4}) predicted from compressive strength and pulse velocity by Equations 11 and 12,
$\overline{X}_j$ = the mean value of X_j, and
X_j^j = the value given by Equation 10 with a = 1, b = 3/2 and c = 3/4.

(2) Using the value of F found in step (1), the coefficients, A_j', were computed from the formula,

$$A_j' = FA_j \tag{14}$$

where A_j is defined in step (1).

This method of transforming the set, A_j, to the set, A_j', preserved the ratios of the coefficients (except ratios involving A_6), and insured that the regression surface defined by the A_j' would - like the surface defined by the A_j - pass through the mean of the data. The transformation was made at some sacrifice in prediction accuracy, but achieved a gain in logic.

The value of F, computed from Equation 13, was 0.9342. Values of A_j', computed from Equation 14, are given in Table 8. The new prediction equation can be formed by substituting the values of the A_j' in Equation 9, and giving values of 1, 3/2 and 3/4 to the constants a, b and c in Equation 10. By making these substitutions in Equations 9 and 10 we obtain Equations 15 and 16, below.

$$W_{ik} = \sum_{j=0}^{7} A_j' X_{ijk} \tag{15}$$

where

$$X_{ijk} = \frac{1}{(.75r_i + H_{1jk})^{3/2}} - \frac{1}{(.75\, r_i + H_{2jk})^{3/2}}, \tag{16}$$

and the A_j' have the values given in Table 8.

The prediction error for Equation 15 was 19.7% of the mean value of the observed deflections. This may be compared with the error of 14.3% associated with the coefficients, A_j, given in Table 7.

That the transformed coefficients are related to compressive strength and pulse velocity is shown in Figures 12 and 13. The correlation coefficients corresponding to the plotted data were 0.99 in both cases. The equations for the lines shown in the graphs are given below:

$$\log A' = 0.7911 - 1.3357 \log S \tag{17}$$

$$\log A' = 0.3368 - 5.3766 V \times 10^{-4} \tag{18}$$

Deflection basins predicted by the transformed coefficients are plotted, together with the observed data, in Figures 14A through 14D. No anomalies of predicted shape will be found in these figures. For this reason, the transformed coefficients, A'_j, are believed by these writers to better represent the physical phenomena than the original set of regression coefficients, A_j.

On the basis of the information presented in this section, the writers feel that the first of the two hypotheses stated in Section 4 of this report can be accepted, though future work scheduled in connection with a related research project may provide improved estimates of the relative stiffness of the eight materials.

Attempts to prove the second hypothesis have not, at this writing, been successful, though work directed toward that end is continuing.

TABLE 7

Values of Constants in Equations 9 and 10

Material Index j	Coefficients, A_j, in Equation 9	Material	Comp.* Strength, S (psi)	Pulse** Velocity V (fps)
0	1.555×10^{-1}	Plastic Clay (undisturbed)		
1	1.017×10^{-1}	Plastic Clay (compacted)	22	2412
2	6.793×10^{-2}	Sandy Clay	40	2576
3	3.794×10^{-2}	Sandy Gravel	43	3721
4	4.278×10^{-3}	Crushed Limestone	165	5222
5	2.804×10^{-3}	Crushed Limestone + 2% Lime	430	5448
6	-1.023×10^{-2}	Crushed Limestone + 4% Cement	2270	7309
7	5.679×10^{-4}	Asphaltic Concrete		

Constants in Equation 10: a = 1, b = 3/2, c = 3/4

Root-mean-square-residual in W: 6.44×10^{-5} in.

Mean value of W: 4.50×10^{-4} in.

RMSR as percent of mean: 14.3%

*Compressive strength at 5 psi lateral pressure, from Table 2, Section 3.

**From Table A-1, Appendix A.

TABLE 8

Values of A'_j in Equation 15

Material Index j	Coefficients, A'_j	Material	Comp.* Strength, S (psi)	Pulse** Velocity V (fps)
0	1.453×10^{-1}	Plastic Clay (undisturbed)		
1	9.505×10^{-2}	Plastic Clay (compacted)	22	2412
2	6.346×10^{-2}	Sandy Clay	40	2576
3	3.544×10^{-2}	Sandy Gravel	43	3721
4	3.997×10^{-3}	Crushed Limestone	165	5222
5	2.619×10^{-3}	Crushed Limestone + 2% Lime	430	5448
6	2.102×10^{-4}	Crushed Limestone + 4% Cement	2270	7309
7	5.305×10^{-4}	Asphaltic Concrete		

Root-mean-square residual in W: 8.86×10^{-5} in.

Mean value of W: 4.50×10^{-4} in.

RMSR as percent of mean: 19.7%

*Compressive strength at 5 psi lateral pressure from Table 2, Section 3.

**From Table A-1, Appendix A.

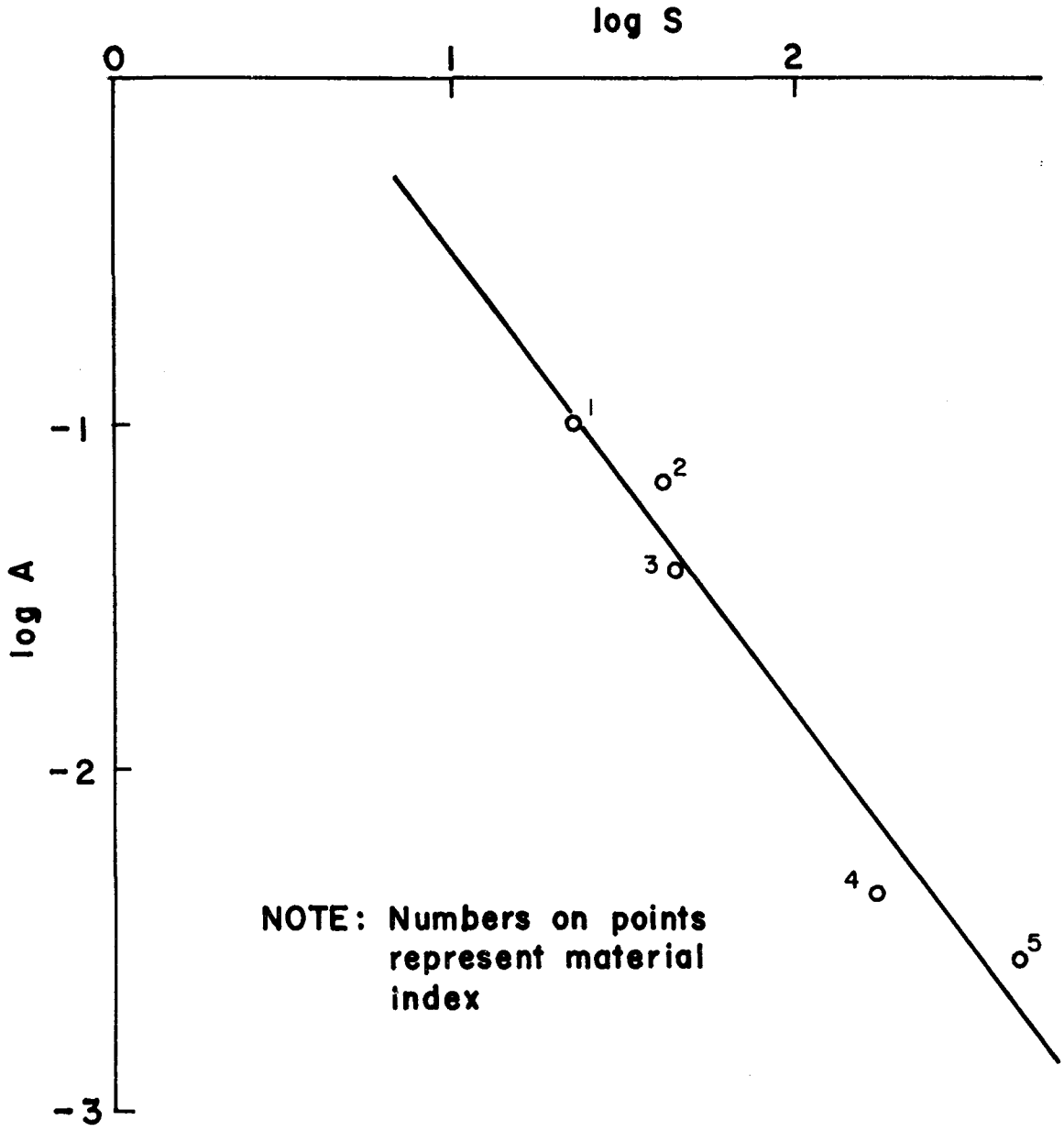

Figure 9: Plot suggesting a functional relationship between the material coefficients, A_j, and the compressive strengths S_j, given in Table 7.

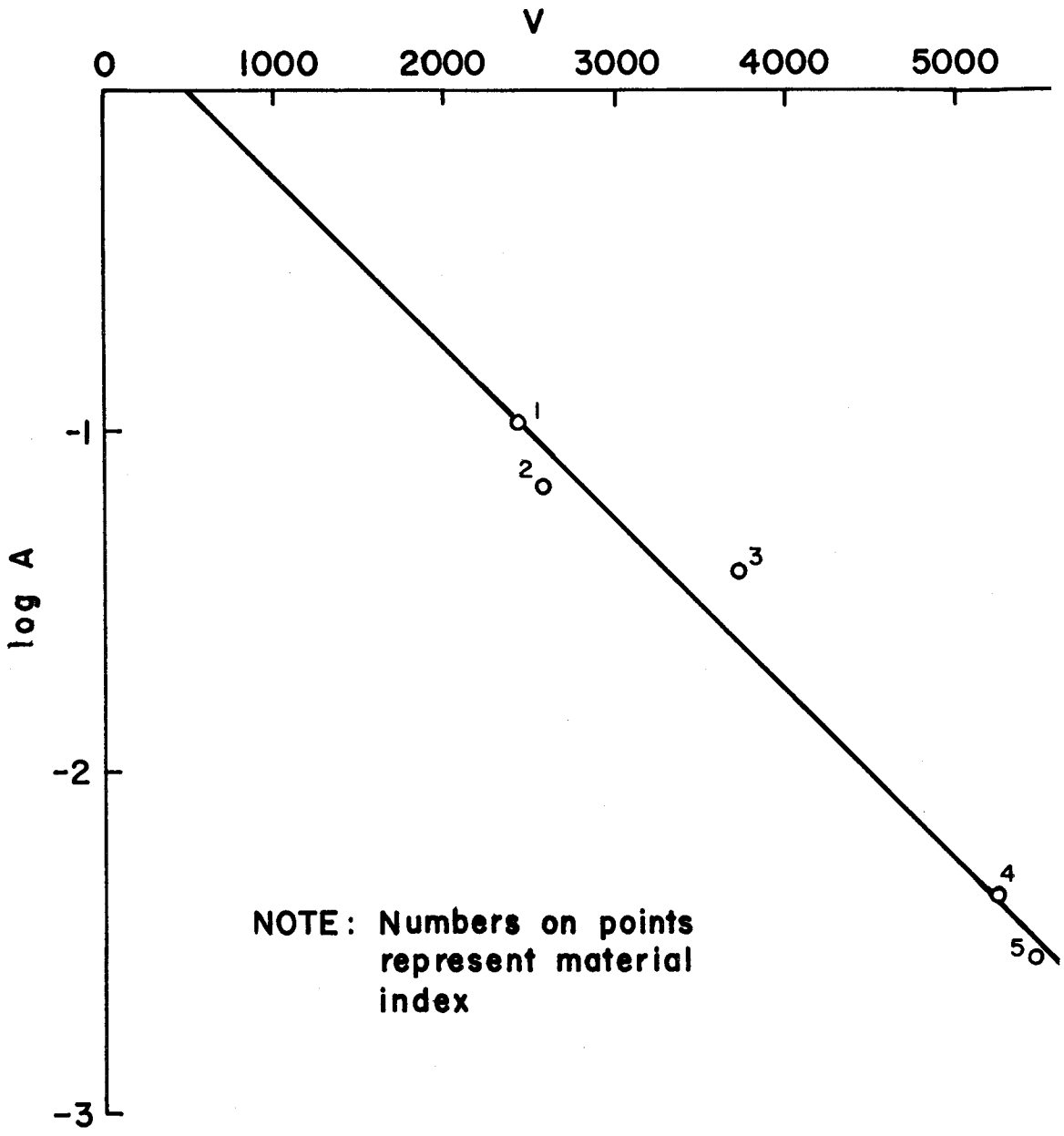

Figure 10: Plot suggesting a functional relationship between the material coefficients, A_j, and the pulse velocities, V_j, given in Table 7.

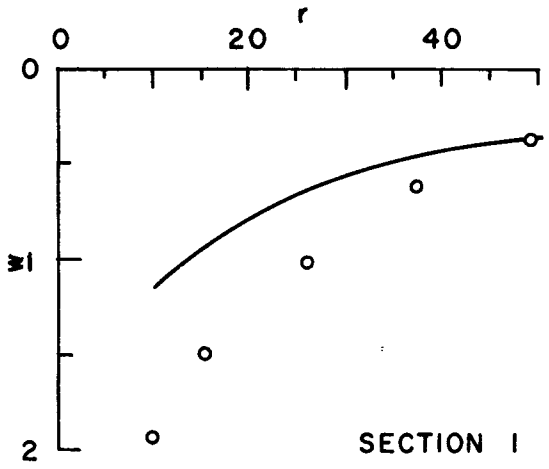

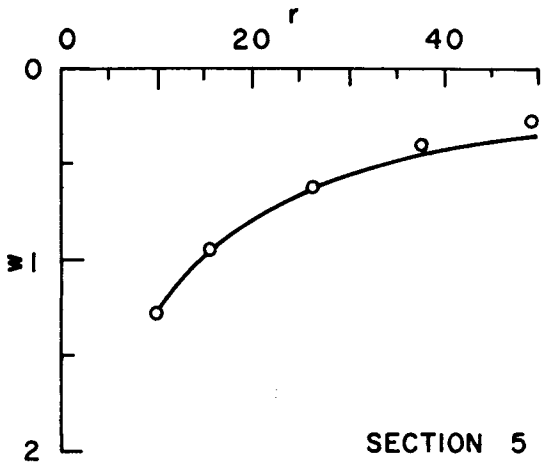

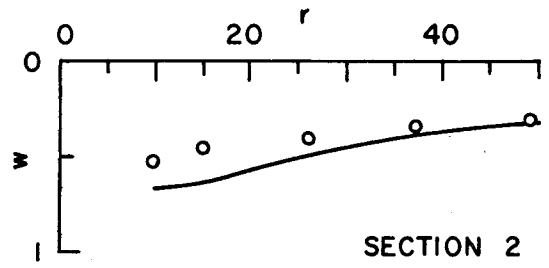

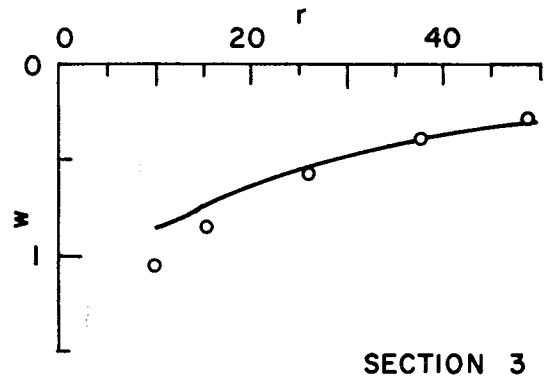

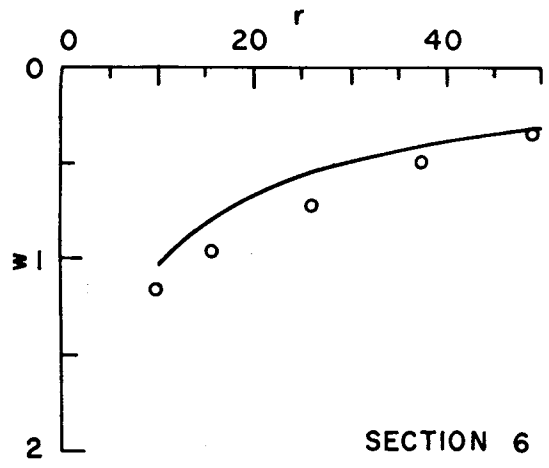

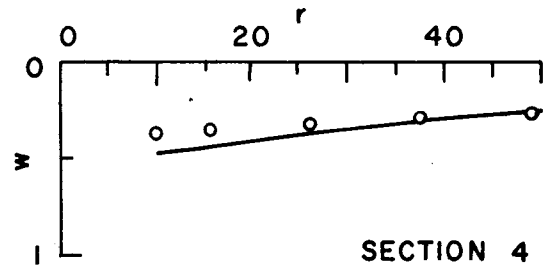

Note: r in inches
w in milli-inches

FIGURE IIA

Observed data (circled points) compared with prediction made from deflection equation. See also Figure IIB through IID.

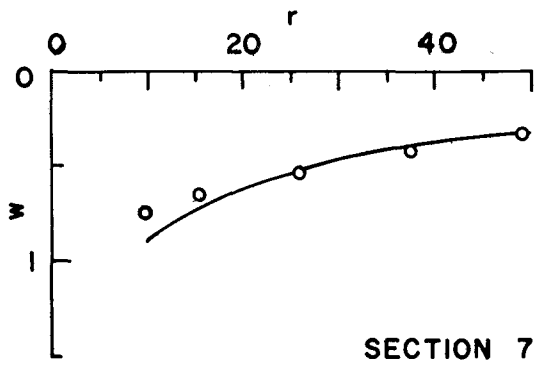

SECTION 7

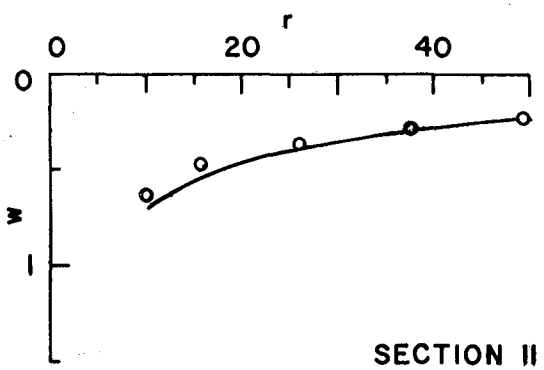

SECTION 11

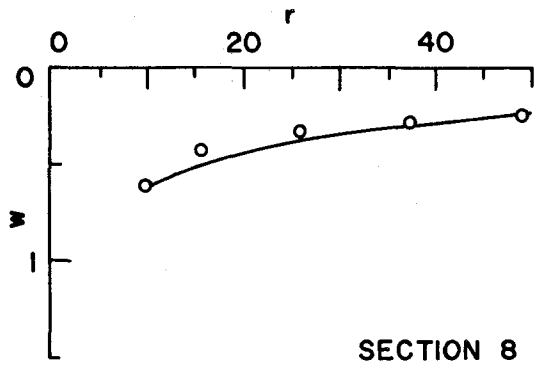

SECTION 8

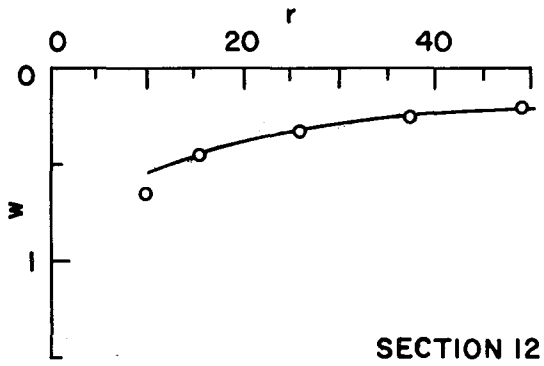

SECTION 12

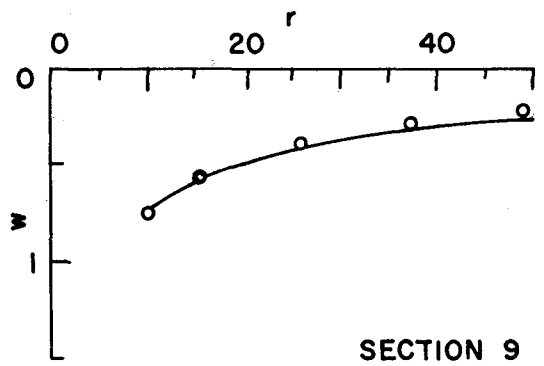

SECTION 9

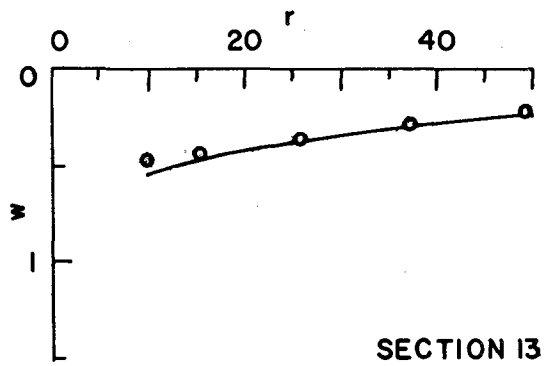

SECTION 13

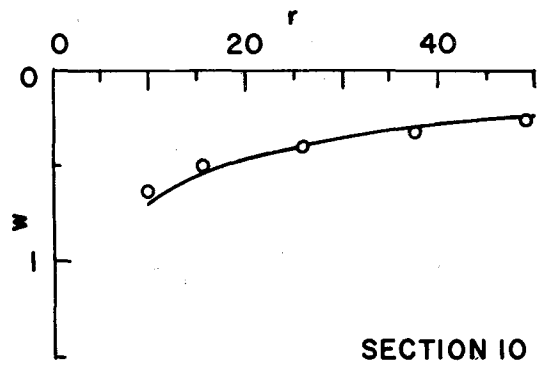

SECTION 10

Note: r in inches
w in milli-inches

FIGURE 11B

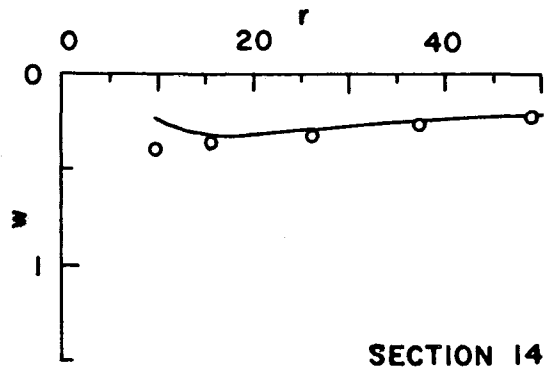

SECTION 14

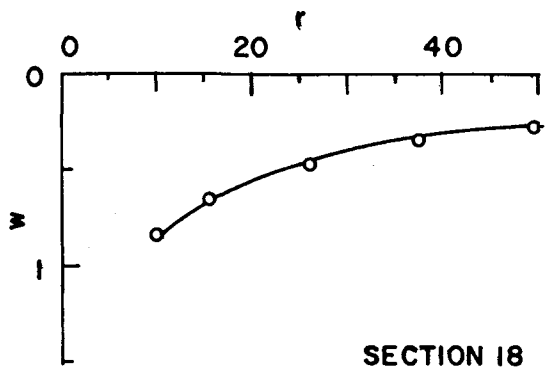

SECTION 18

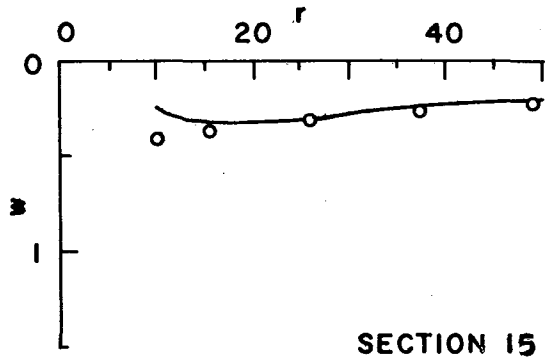

SECTION 15

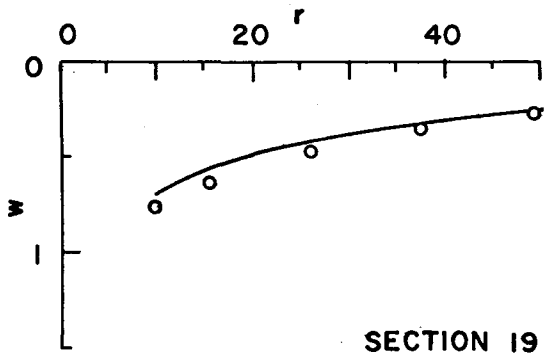

SECTION 19

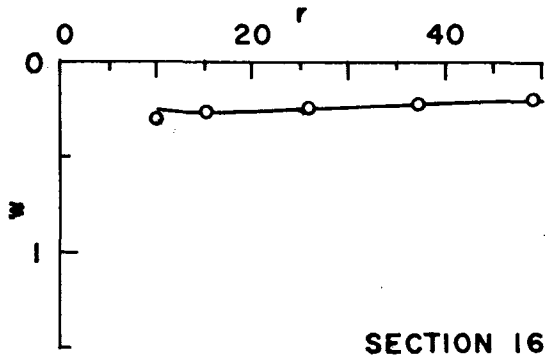

SECTION 16

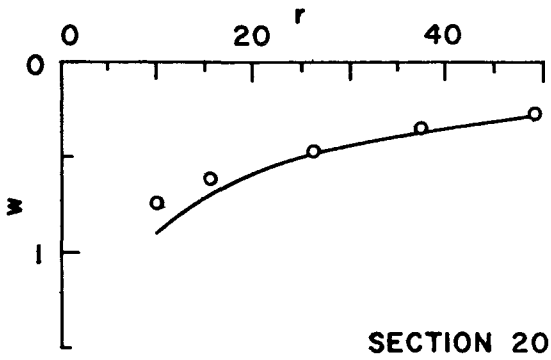

SECTION 20

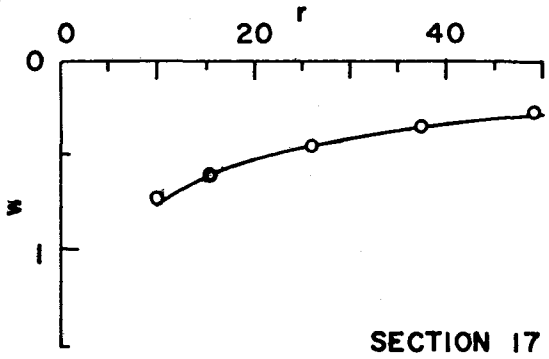

SECTION 17

Note: r in inches
w in milli-inches

FIGURE 11C

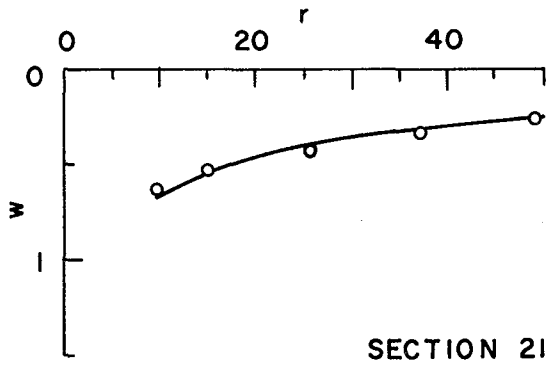

SECTION 21

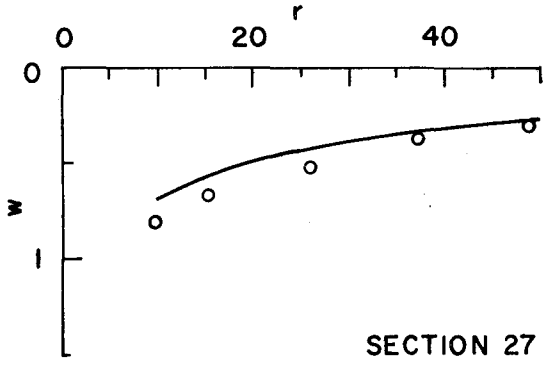

SECTION 27

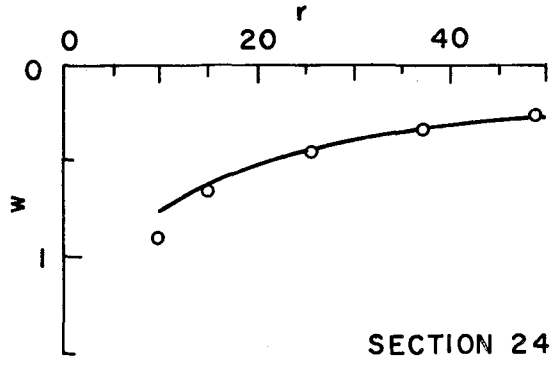

SECTION 24

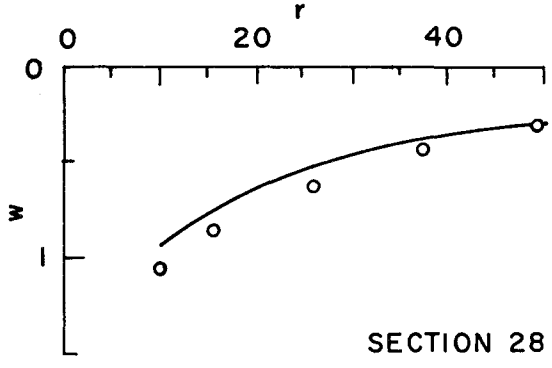

SECTION 28

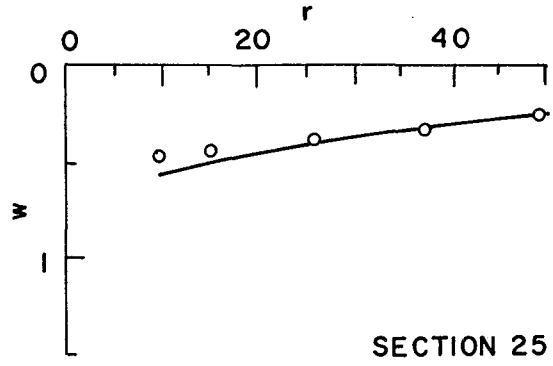

SECTION 25

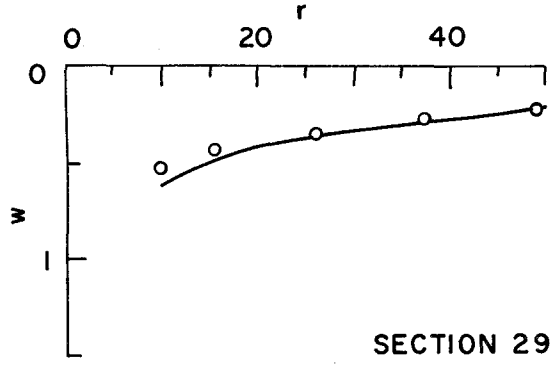

SECTION 29

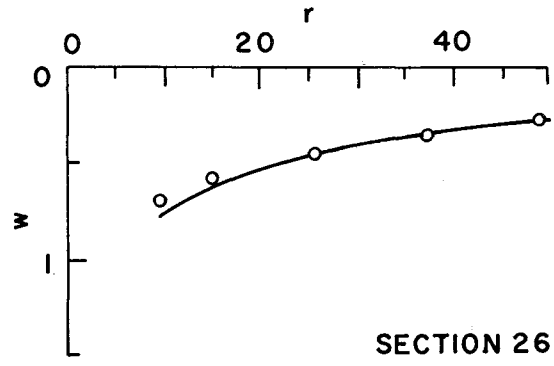

SECTION 26

Note: r in inches
w in milli-inches

FIGURE IID

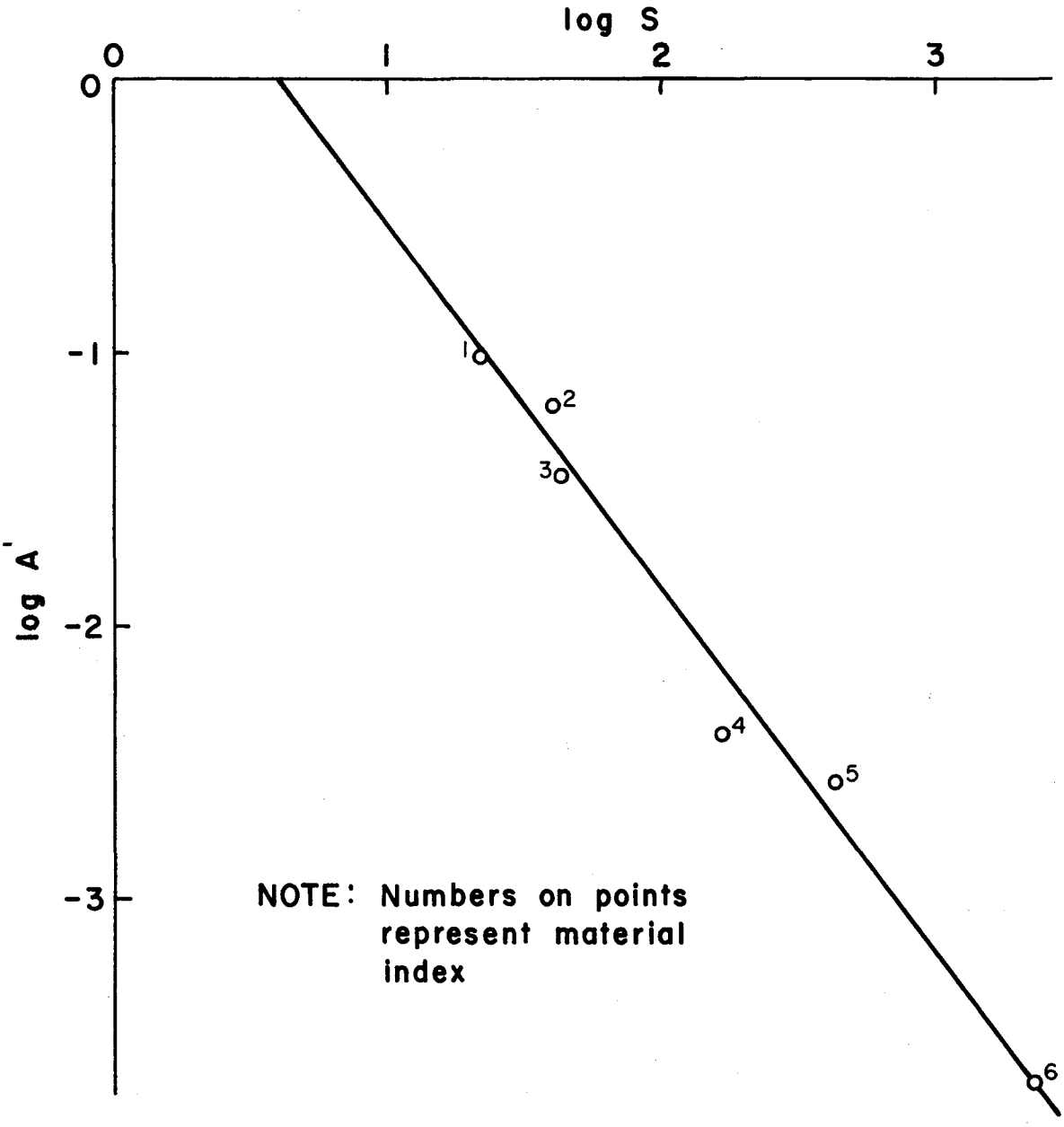

Figure 12: Plot of the adjusted coefficients, A_j', versus the logarithm of compressive strength.

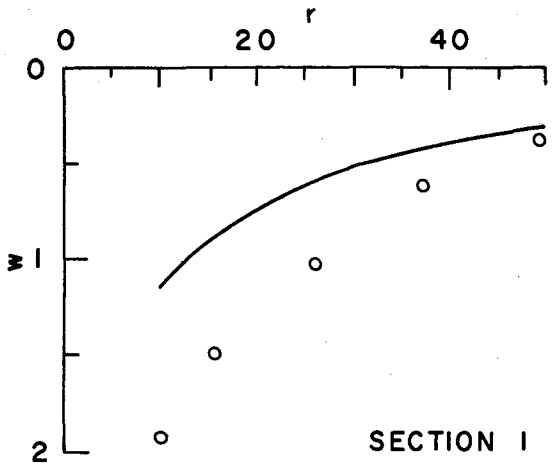

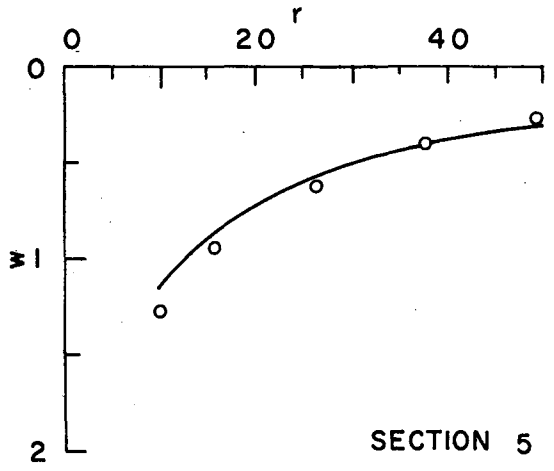

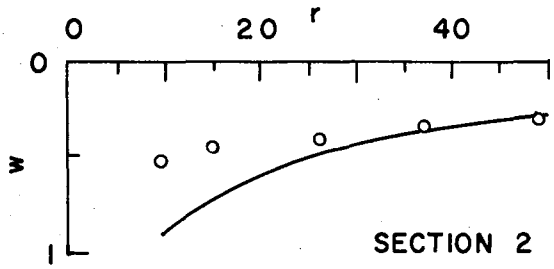

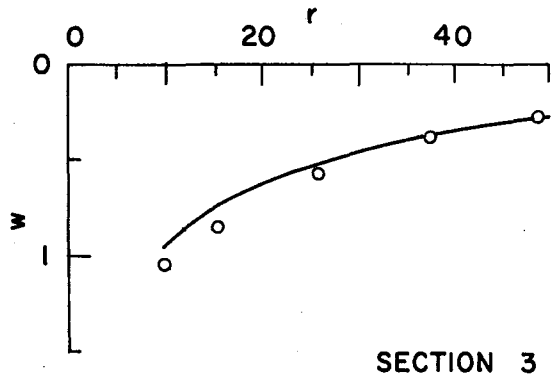

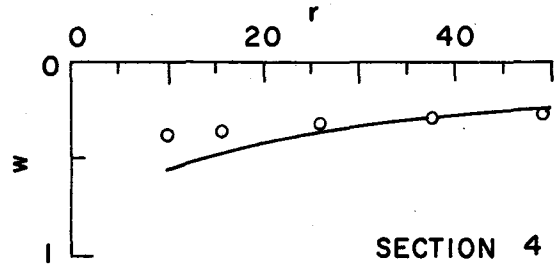

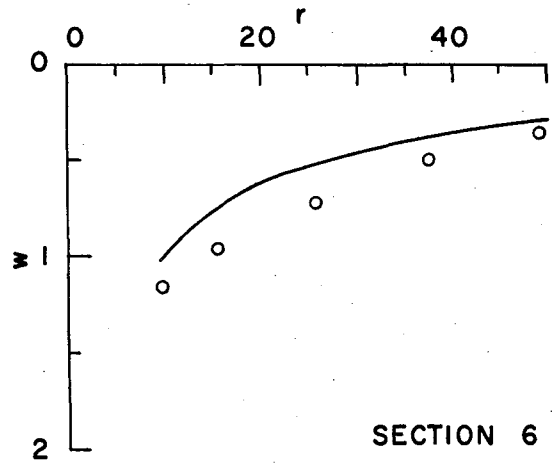

Note: r in inches
w in milli-inches

FIGURE 14A

Observed data (circled points) compared with prediction made from adjusted deflection equation. See also Figure 14B through 14D

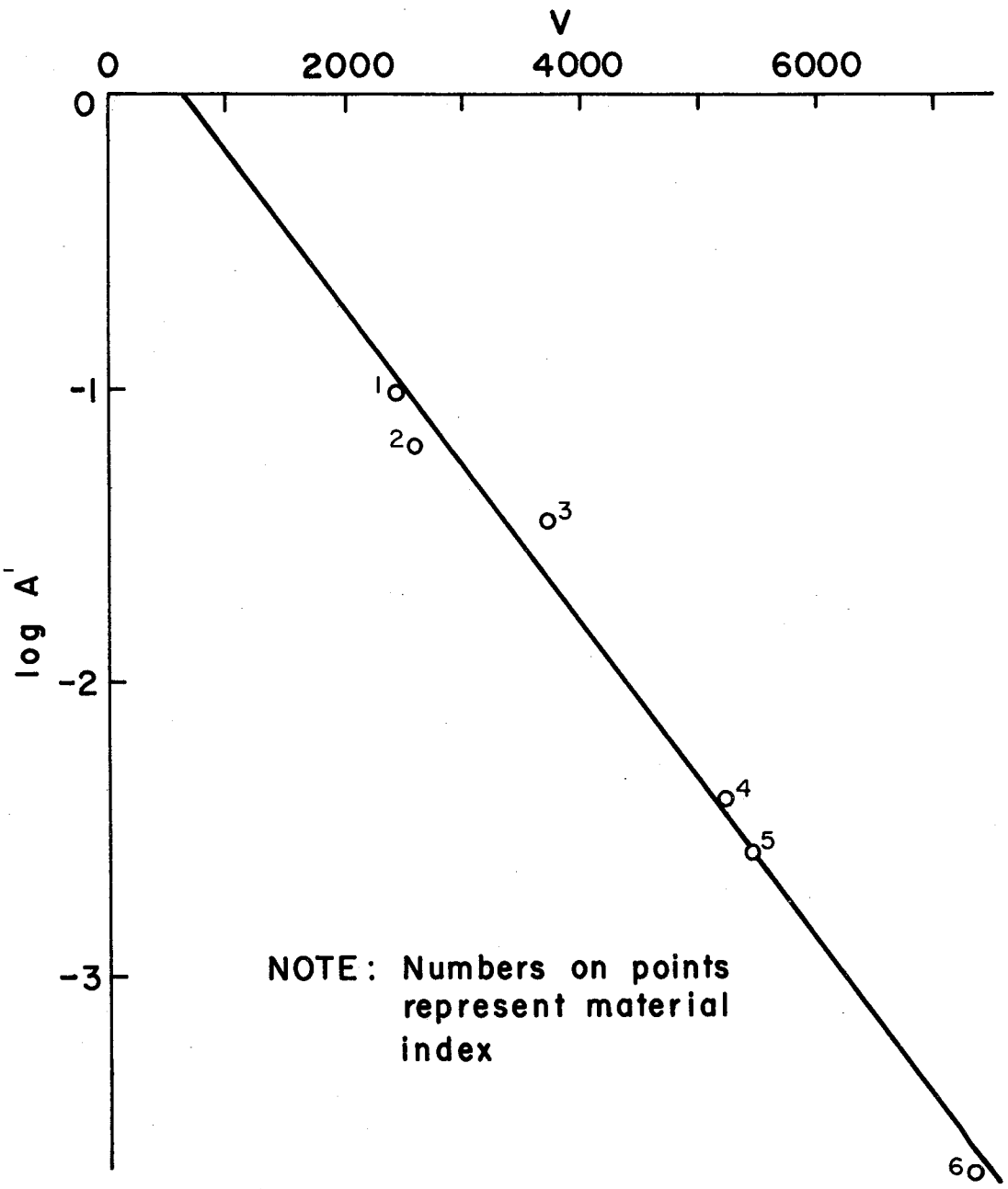

Figure 13: Plot of the adjusted coefficients, A_j', versus pulse velocity.

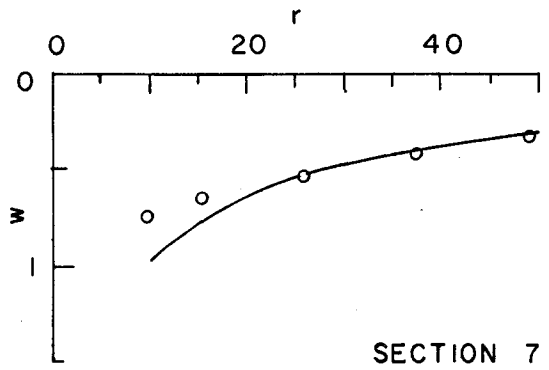

SECTION 7

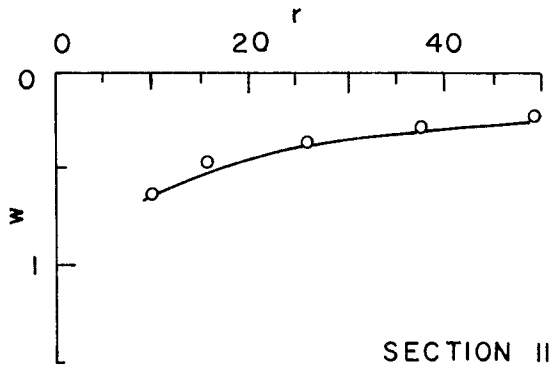

SECTION 11

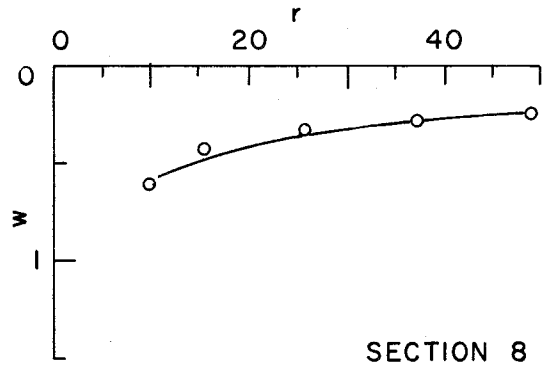

SECTION 8

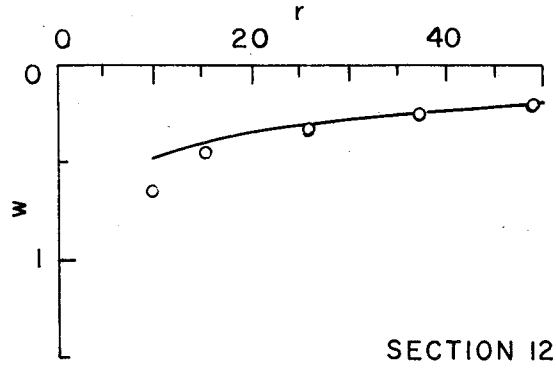

SECTION 12

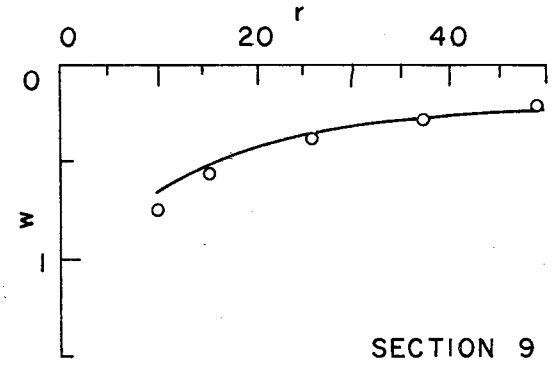

SECTION 9

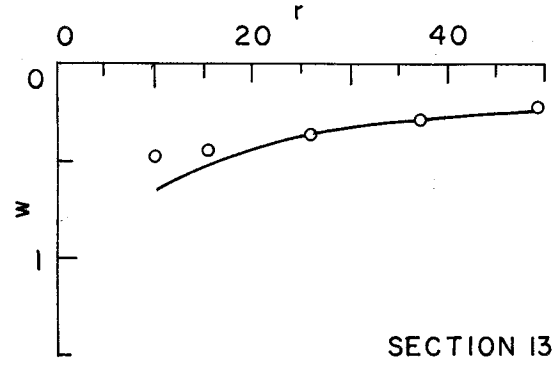

SECTION 13

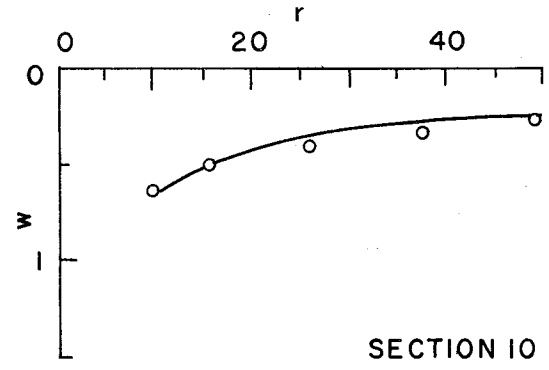

SECTION 10

Note: r in inches
w in milli-inches

FIGURE 14B

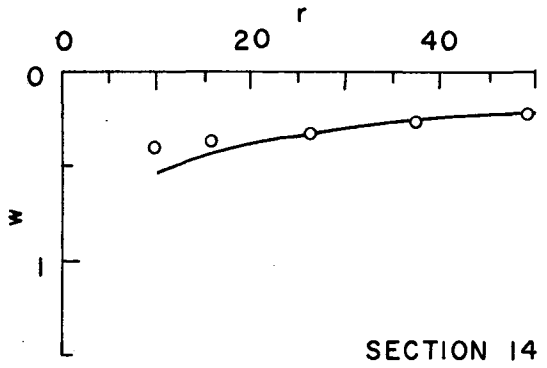

SECTION 14

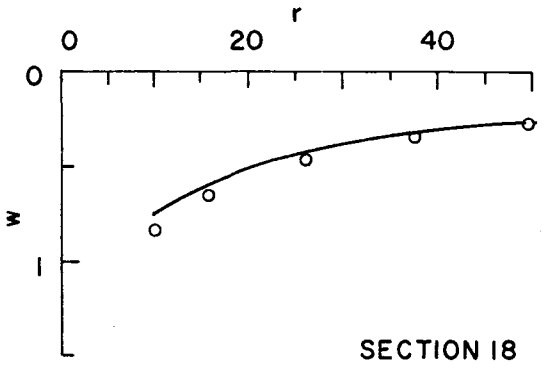

SECTION 18

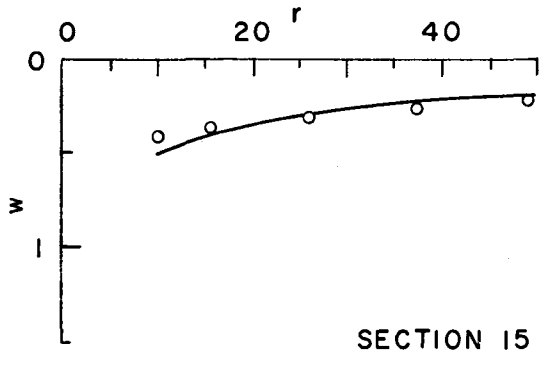

SECTION 15

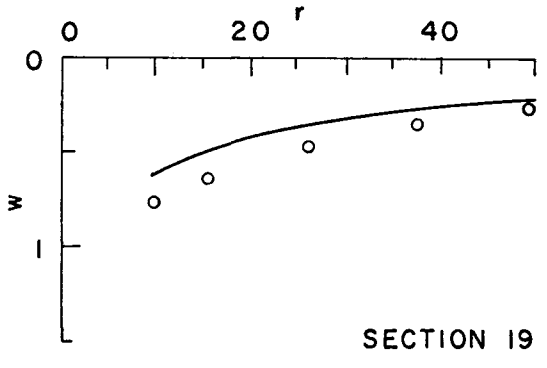

SECTION 19

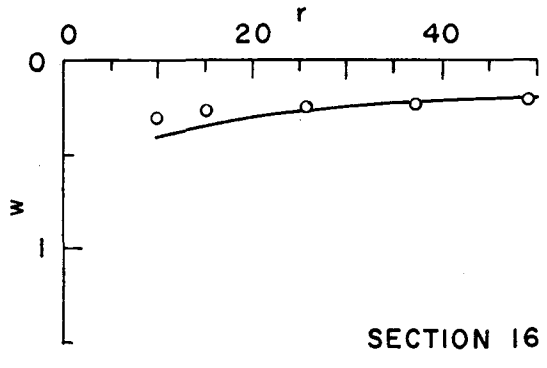

SECTION 16

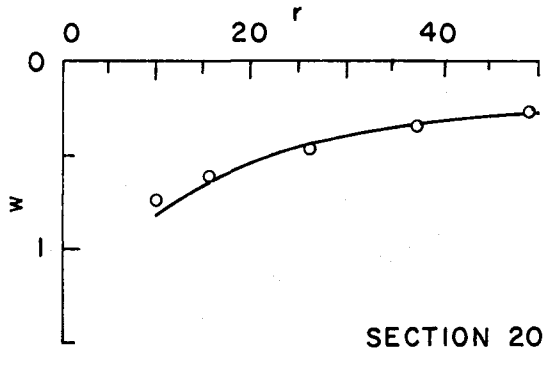

SECTION 20

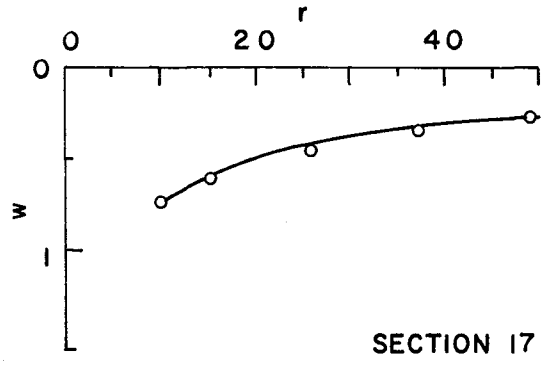

SECTION 17

Note: r in inches
w in milli-inches

FIGURE 14C

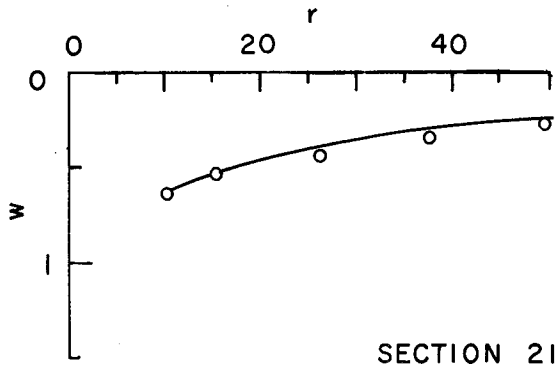

SECTION 21

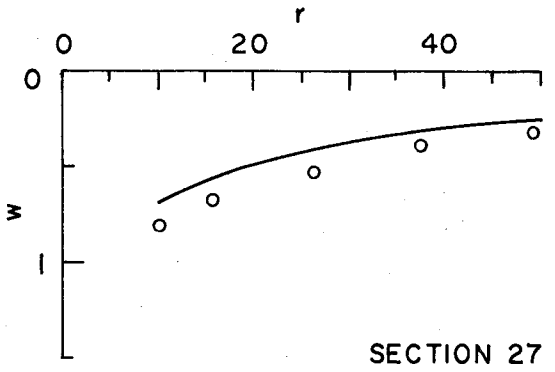

SECTION 27

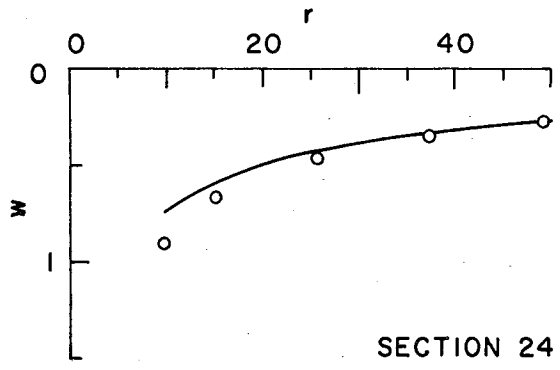

SECTION 24

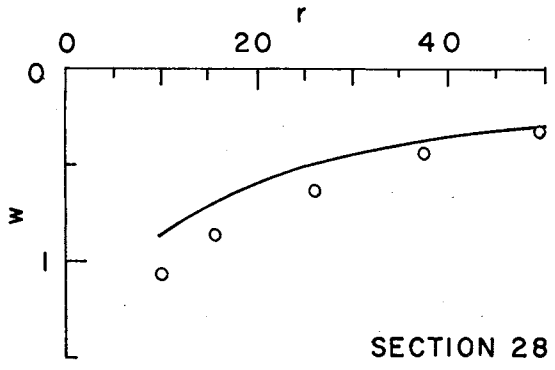

SECTION 28

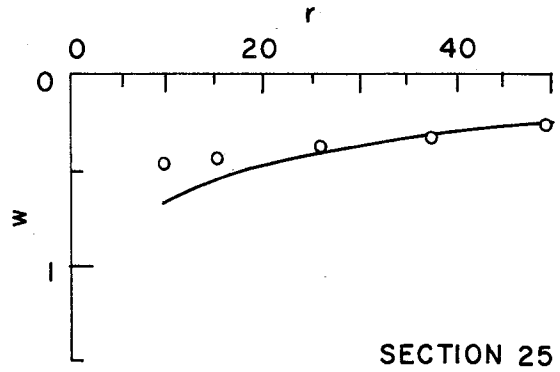

SECTION 25

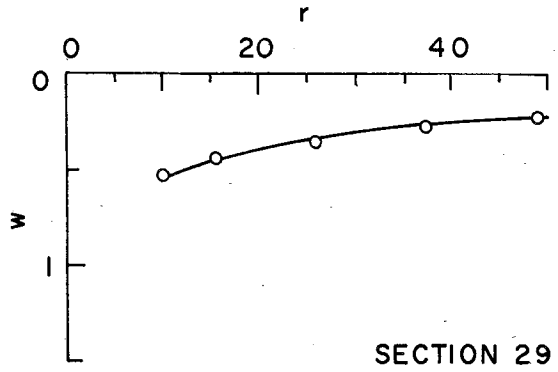

SECTION 29

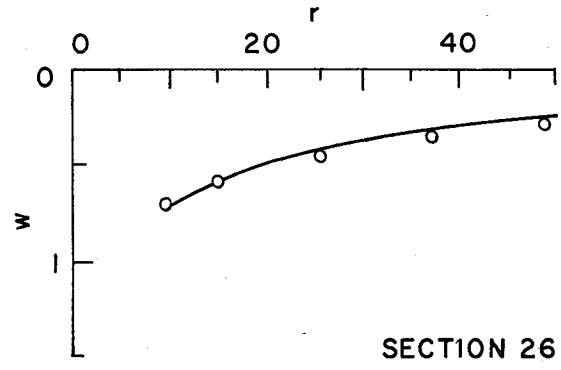

SECTION 26

Note: r in inches
w in milli-inches

FIGURE 14 D

APPENDIX A

SEISMIC TESTS

In recent years seismic methods of testing materials have received considerable attention. It has been observed that the velocity of propagation of the compressional wave alone provides some information about the physical characteristics of a given material. If the velocity of the shear wave in a material as well as the compressional wave are known, then its elastic constants may be calculated (provided, of course, the material deforms in accordance with Hooke's Law).

In this work primary importance was attached to determining the compressional velocity of each of the materials used in the construction of the test facility. (The more difficult problem of determining the shear velocities of the materials was also attempted, but the results obtained were not conclusive.)

Two methods were used to measure the seismic velocities. A brief discussion of each method follows.

One of the methods is generally referred to as a "pulse technique" or "ultrasonic technique". In order to best describe this method, mention should be made of the apparatus used. The apparatus (Figure A-1), assembled at Texas Transportation Institute, consisted of four major components: a pulse generator, a source transducer, a receiver transducer, and an oscilloscope. The pulse generator actuates the source transducer (a ceramic piezoelectric crystal) and triggers the horizontal sweep of the oscilloscope. Actuation of the source transducer causes seismic energy to be transmitted through the sample to the receiver transducer (another ceramic piezoelectric crystal). The output of the receiver transducer is displayed on the horizontal sweep of the oscilloscope. A time delay device built into the oscilloscope is used to make the arrival of the seismic energy at the receiver transducer coincide with the start of the horizontal sweep. The time required for the seismic energy to travel through the sample may then be read directly from the time delay device. Knowing the length of the sample, the seismic velocity may be determined.

This method is generally used to measure seismic velocities in cores or prepared samples. However, its use was extended in this work to testing the material in situ as well. This was accomplished by digging small holes, in which were placed the source and receiver transducers, to measure the velocity along a path parallel to the road surface.

In order to have an independent method of measuring velocities, so that a comparison could be made with the values obtained from the pulse technique, measurements were made with a portable seismograph. The seismograph used was a multi-channel instrument manufactured by Geo Space Corporation in Houston, Texas, and marketed as the Geo Space GT-2 Portable Seismograph. This unit is designed for shallow refraction studies which might be encountered in foundation design, ground water studies, and other problems where the layers of interest are several feet or tens of feet thick.

Measurements were made with the seismograph on each section, as each component of the test facility was completed. The procedure was to lay out six geophones at intervals of five feet along a line parallel to the long axis of the section (Figure A-2) with which to record the seismic energy from the source, a hammer blow using a steel plate as a coupler. The seismograph provided a Polaroid picture, from which the time required for the energy to travel from the source to each geophone could be read. Then knowing the distance to each geophone, and assuming that the energy traveled directly from source to geophone, the velocity of the wave front could be determined at each of the six geophones. However in practice these values were averaged by taking the velocity to be the inverse of the slope of the best fit line drawn through the points on a graph where time of travel is plotted as ordinates against distance from the source (Figure A-3).

The seismometers, designed to measure motion in a plane horizontal to the earth's surface, were oriented such that they would measure motion in the direction of propagation of the seismic energy. This orientation was chosen because elastic theory predicts that this should be the direction of particle motion for a compression wave.

Table A-1 gives a summary of the results of the compressional velocity measurements made by both the portable seismograph and the pulse technique. In situ measurements were made during construction at a time when the lime and cement stabilized materials had not completely cured. Thus the velocities measured in these materials were probably less than the ultimate attained after curing.

According to Table A-1 the velocities determined by the two methods for the same material do not show the agreement that was expected. This lack of agreement is too great to be attributed to experimental error in either method; therefore, one must seek an explanation in the basic assumptions of the methods. Before considering the assumption of both methods it should be mentioned that although the velocities obtained by the two methods show poor agreement, the velocities were consistent in the sense that for a given material the velocity determined by the pulse technique was always greater than that determined by the portable refraction device. Any satisfactory explanation must be in accord with this fact.

The use of the pulse technique to determine compressional velocity has been well founded by many previous investigators--Leslie, Jr. R. (1950)[6], Birch, F. (1960)[7] and others. This, together with the fact that we could find no plausible reason why this method would not give the correct values, caused us to accept these values as being close to the true compressional wave velocities. Thus, to explain the discrepancy between the velocities obtained by the two methods, we must consider the measurements made with the portable refraction seismograph.

The measurements made with the portable refraction device were made on the top of each component as the test facility was constructed. As the tests

were made on the top of a component just completed, it was assumed that the velocity measured would be the compressional velocity of the material in that particular component, if the underlying materials exhibited lesser velocities.

The average compressional velocity of each of the materials determined by this procedure are given in Table A-1; however, measurements made on top of the base in Sections 5, 6, 7, 8, 24 and 27 were excluded since according to Table 3, the stiffness of the base materials in these sections was judged to be less than the subbase materials beneath them. Also the measurements made on the top of the asphalt are not included, but are given separately in Table A-2, as the velocity measured appears to be primarily influenced by the material of the base and subbase.

In Table A-2 the velocities measured on the top of the asphalt are grouped according to the material of the base and subbase. In each of the groups the average surface thickness is 3 inches and the average base and subbase thickness 8 inches; therefore the differences in the average velocities are apparently due to the base and subbase materials underlying the asphaltic concrete.

The assumption made in determining the velocities was tantamount to assuming that "ray theory" seismology was valid. In ray theory seismology, the rays (or perpendiculars to the wave fronts) are assumed to obey Snell's Law and from this one is able to make predictions concerning the path the seismic energy will take if the elastic constants of the medium are known. The theory of refraction seismology, as it is used in studies of the earth (considering the earth as a layered media), is based on a particular ray of an infinite number of rays. This ray is called the "critical angle ray", and is defined by the following equation:

$$\text{sine } ic = \frac{V_1}{V_2} \quad , \tag{1}$$

where V_1 and V_2 are compressional wave velocities of layer 1 and 2 respectively (Figure A-4), ic is the critical angle and $V_2 > V_1$. Figure A-4 shows the path the energy appears to follow for this special case as well as the path for the direct wave. Figure A-5 is a theoretical travel time plot (where the time of travel for the first arriving energy is plotted against the distance from source to receiver) for the layering of Figure A-4. The travel time plot shows that from the source out to some particular distance X_c (called the critical distance) the direct wave arrives first, but past that distance the refracted wave arrives first even though it travels a greater distance. The reason for this is that it travels at a greater velocity (V_2) through the segment (BC) of its path. The velocity of each layer is equal to the inverse of the slope of the corresponding segment of the travel time plot.

The critical angle refraction technique has been widely used in earth studies, and has provided much useful information. An important character-

istic of this method becomes apparent if you consider Equation (1) in the light of having a velocity V_2 less than V_1. This results in the sine of ic being greater than unity, an impossibility. Therefore there will be no critical angle for a layer with a velocity less than any layer above it, and this method will provide no information about such a layer. Thus, if ray theory were valid and the material on which the tests were made had a greater velocity than any material beneath it, the velocity measured should be that of the material on which the test was made. The results of the experiment have caused us to doubt the validity of this assumption. It now appears likely that ray theory was not valid and that this was the cause of the poor agreement of the two methods. It is our belief that ray theory was inadequate for this study because the wave length of the first recorded energy at each geophone was much larger than the thickness of the components in the test facility.

An examination of the records from the portable seismograph showed that a value of .005 second would be a reasonable minimum value for the period (t) of the first arriving energy. If one considers a velocity of 1000 ft./sec., which is very low, and assumes the following relation to be valid:

$$\lambda = vt \qquad (2)$$

this would predict a wave length of 5 feet as a minimum. It appears likely to us that having a wave length much larger than the thickness of the components would result in the wave traveling in the material below the component as well as in the component itself. This would cause any measured velocity in Table A-1 to be less than the actual velocity of the component on which the measurements were made, a result that satisfies the criteria mentioned previously concerning the relation between the velocity determined by the pulse technique and the portable refraction seismograph.

From the results of this work it seems unlikely that a "typical" portable refraction device designed for general engineering purposes would be an adequate tool for determining directly the compressional wave velocities in individual structural components of flexible pavements, because such an instrument is not designed to initiate and detect the high frequency short wave length energy apparently required for this application. However, Phelps and Contor (1966)[8], reported using successfully the seismic refraction technique to determine the velocity of thin layers of asphalt overlying concrete. They used a recording system which was much more sensitive to higher frequencies, much shorter intervals between the energy source and detectors, and a less energetic source. With this specialized instrumentation, the seismic refraction technique might be a useful tool for testing highway construction materials.

TABLE A-1

Compressional Velocities
by Two Methods

Material Index	Where Used	Description	Pulse Technique						Portable Seismograph		
			Vel. (fps) Lab.*	No. Obs.	Std. Dev.	Vel. (fps) field**	No. Obs.	Std. Dev.	Vel. (fps) field**	No. Obs.	Std. Dev.
0	Foundation	Plastic Clay (undisturbed)	1744	5	304	--	--	--	1180	7	81
1	Embankment	Plastic Clay	3492	2	430	2412	12	274	1460	10	39
2	Embankment	Sandy Clay	2370	3	265	2576	24	523	1435	20	98
3	Embankment	Sandy Gravel	--	--	--	3721	21	1423	1714	11	190
4	Base & Subb	Cr. Limestone	--	--	--	5222	3	574	2920	12	305
5	Base & Subb	Cr. Limestone + 2% Lime	--	--	--	5448	2	16	2833	19	543
6	Base & Subb	Cr. Limestone + 4% Cement	--	--	--	7309	3	701	5436	22	1074
7	Surfacing	Asph. Conc.	8463	8	208	--	--	--	(See Table #2)		

*Tests made on cores obtained during construction. Asph. conc. core tested at 70^0 F.

**Tests made during construction. Stabilized materials had not completely cured.

TABLE A-2

Compressional Velocities Measured on Top of

Asphalt Surface Layer

Sec No.	Material		Avg. Vel.	No. Obs.	Std. Dev.
	Base	Subbase			
9-12	Cr. Limestone	Cr. Limestone	2990	4	307
17-23, 28-29	Cr. Limestone + 2% Lime	Cr. Limestone + 2% Lime	3480	7	202
5-8	Cr. Limestone	Cr. Limestone + 4% Cement	4928	4	1210
1-4	Cr. Limestone + 4% Cement	Cr. Limestone	6615	4	778
13-16	Cr. Limestone + 4% Cement	Cr. Limestone + 4% Cement	7513	4	920

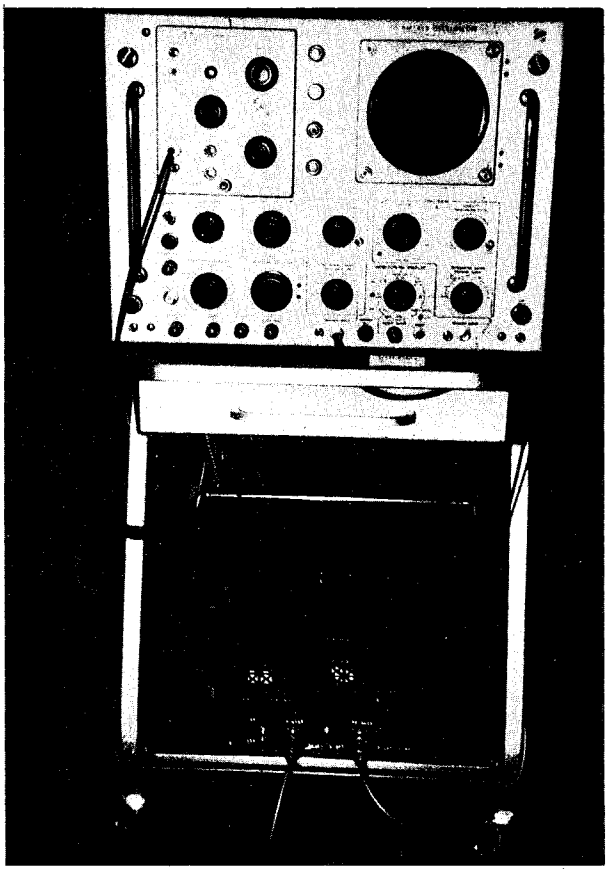

Figure A-1: Oscilloscope and pulse generator on mobile cart.

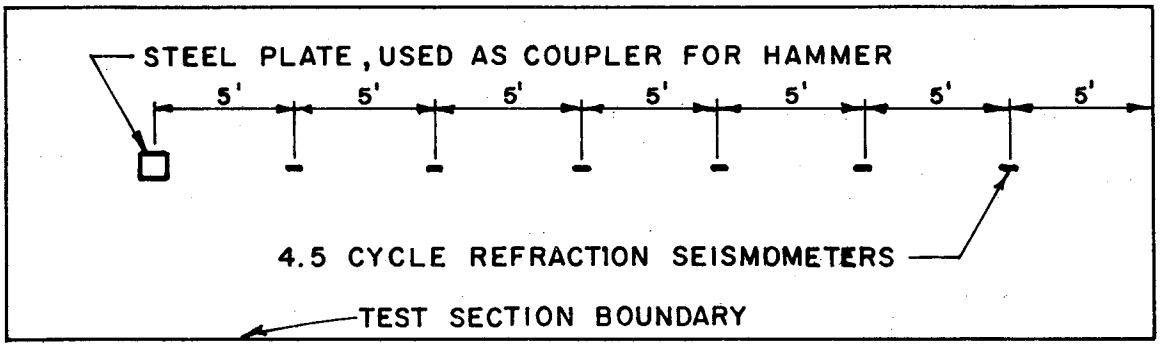

Figure A-2: Seismometer arrangement used to determine compressional wave velocity.

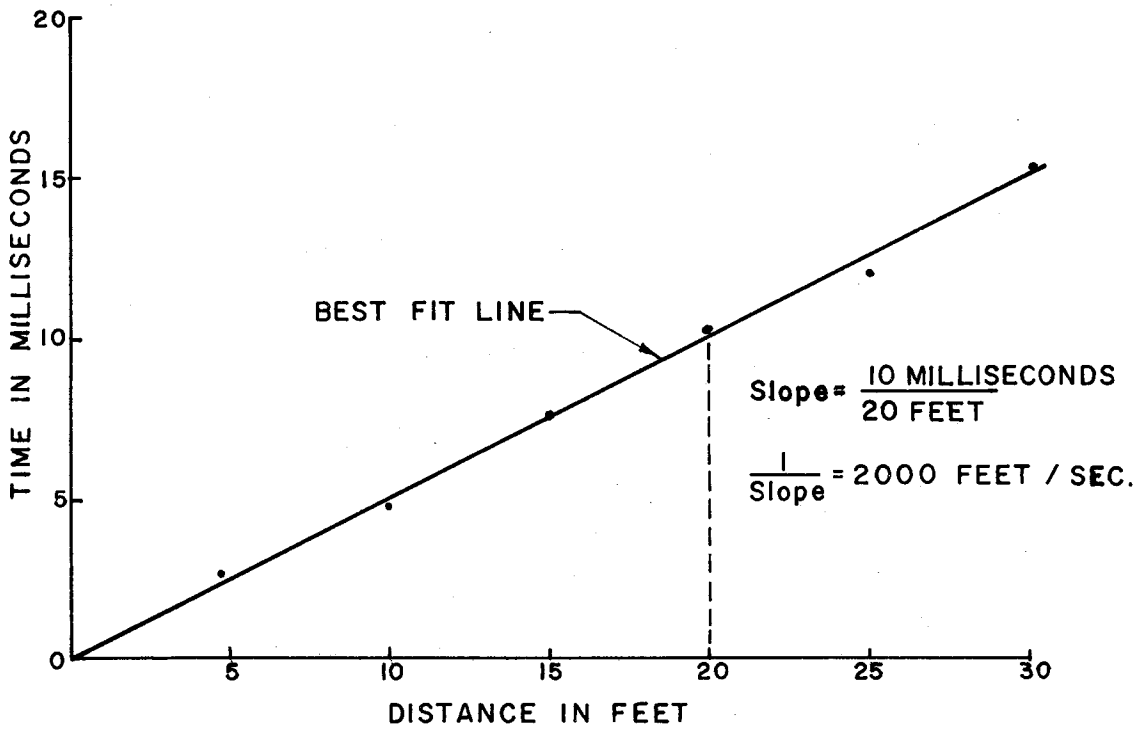

Figure A-3: Travel time plot for energy traveling direct path from source to geophones.

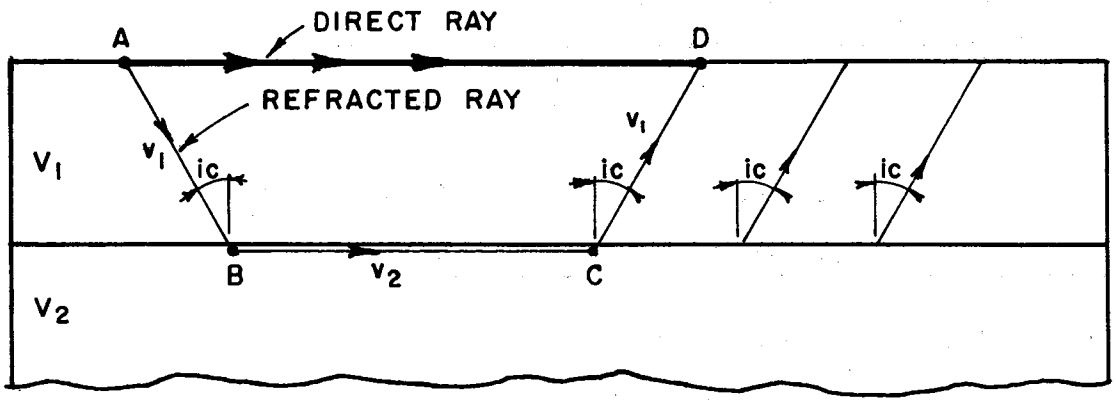

Figure A-4: Ray path for critical angle ray and direct ray.

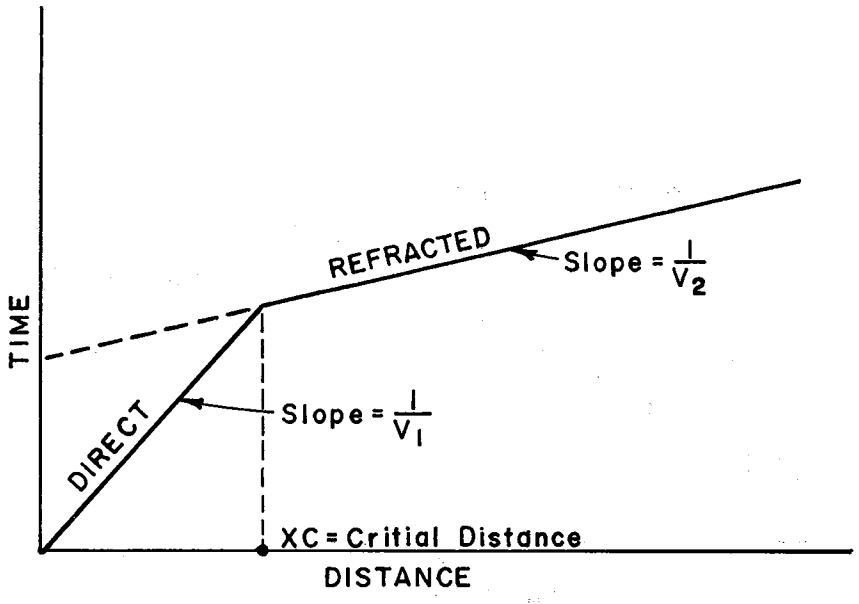

Figure A-5: Theoretical travel time plot for two layer critical angle refraction.

APPENDIX B

(REPORT V)

MULTIPLE ERROR REGRESSION TECHNIQUE

B-1. INTRODUCTION

In the classical least-squares method of fitting a linear model to data collected in an experiment involving several variables, it is assumed that the values of all but one - the dependent or response variable - are known precisely. Frequently, however, there are errors of measurement in all the variables, and when this is the case the classical method yields a biased estimate of the regression coefficients. Since the objective of most experiments is to obtain unbiased estimates of these coefficients, it is apparent that measurement errors in the independent variables should not be ignored.

The regression technique described herein accounts for errors in all variables. It is essentially the same as a method described by J. Johnston,[9] but includes a new concept - that of the "quality" of a variable. Because of the introduction of this concept, and because it was desired to confirm Johnston's results by independent means, it was necessary to perform the mathematical operations described in the following sections.

The reader who does not desire to follow the derivations will find the gist of the method in Sections 5, 6, 7 and 8.

B-2. ASSUMPTIONS

Let it be supposed that an experiment involves a set of p variables, the true values of which are known to be linearily dependent. We name the variables $X_1, X_2, \ldots, X_j, \ldots, X_p$.

In the course of the experiment we measure the whole set of variables from time to time (or from place to place, depending on the nature of the experiment). At one of these times (or places) we obtain the ith set of measurements, $X_{i1}, X_{i2}, \ldots, X_{ij}, \ldots, X_{ip}$.

Corresponding to the ith set of measurements, there is a set of true values, $\tilde{X}_{i1}, \tilde{X}_{i2}, \ldots, \tilde{X}_{ij}, \ldots, \tilde{X}_{ip}$, and a set of measurement errors, $e_{i1}, e_{i2}, \ldots, e_{ij}, \ldots, e_{ip}$.

We assume that the measurement errors are random, independent, and normally distributed, with a mean value of zero. The measurement error, e_{ij}, is defined by

$$X_{ij} = \tilde{X}_{ij} + e_{ij} \quad . \tag{1}$$

The true values of the variables, according to our assumption of linear dependence, satisfy the equation

$$A_o + \sum_{j=1}^{p} A_j \tilde{X}_{ij} = 0 \quad , \tag{2}$$

where $A_o, A_1, \ldots, A_p$ are constants.

B-3. DERIVATION OF EXPRESSION TO BE MINIMIZED

Equations 1 and 2 lead directly to a relationship involving the measured values and measurement errors, as follows:

$$A_o + \sum_{j=1}^{p} A_j X_{ij} = \sum_{j=1}^{p} A_j e_{ij} \quad . \tag{3}$$

By squaring Equation 3 and then summing over the index i, we obtain,

$$\sum_{i=1}^{n} (A_o + \sum_{j=1}^{p} A_j X_{ij})^2 = \sum_{i=1}^{n} (\sum_{j=1}^{p} A_j e_{ij})^2 \quad , \tag{4}$$

where n is the total number of times the set of variables has been measured.

We may simplify Equation 4 somewhat by eliminating A_o, as indicated below.

Noting that the error term is independent of A_o, we differentiate Equation 4 with respect to A_o, and solve the resulting equation for A_o, obtaining

$$A_o = -\frac{1}{n} \sum_{i=1}^{n} \sum_{j=1}^{p} A_j X_{ij} \quad ,$$

or, more briefly,

$$A_o = -\sum_{j=1}^{p} A_j \bar{X}_j \quad , \tag{5}$$

where $\bar{X}_j$ is the mean of the n measured values of the variable X_j.

By substituting the right side of Equation 5 for A_o in Equation 4, we obtain an equation in terms of the deviations of the measured variables from their means:

$$\sum_{i=1}^{n} (\sum_{j=1}^{p} A_j V_{ij})^2 = \sum_{i=1}^{n} (\sum_{j=1}^{p} A_j e_{ij})^2 \quad , \tag{6}$$

where $V_{ij} = X_{ij} - \bar{X}_j$ = the deviation of X_{ij} from the mean of the n measured values of X_j.

The right side of Equation 6 can be expanded into the sum of a series of terms of the type

$$A_j A_k \sum_{i=1}^{n} e_{ij} e_{ik} \quad .$$

But, for large n, every term for which $j \neq k$ has an expected value of zero as a consequence of our previously stated assumption regarding the measurement errors, e_{ij}. If we neglect terms for which $j \neq k$, there will remain in the series only terms of the type,

$$A_j^2 \sum_{i=1}^{n} e_{ij}^2 \quad (j = 1, \ldots, p).$$

Thus, Equation 6 may be written in the following form:

$$\sum_{i=1}^{n} \left(\sum_{j=1}^{p} A_j V_{ij} \right)^2 = A_1^2 \sum_{i=1}^{n} e_{i1}^2 + \ldots + A_p^2 \sum_{i=1}^{n} e_{ip}^2 \quad . \tag{7}$$

Without loss of generality, we separate each constant, A_j, into two arbitrary factors, C_j and M_j, and define one of the factors as indicated below:

$$A_j \equiv C_j M_j \quad , \tag{8}$$

where M_j is defined by

$$M_j \equiv \left[\sum_{i=1}^{n} e_{ip}^2 \Big/ \sum_{i=1}^{n} e_{ij}^2 \right]^{1/2} \quad . \tag{9}$$

We also introduce a new variable, Z_{ij}, defined by

$$Z_{ij} \equiv M_j V_{ij} \quad . \tag{10}$$

From Equations 8 and 10 it can be seen that

$$A_j V_{ij} = C_j M_j V_{ij} = C_j Z_{ij} \quad . \tag{11}$$

From Equations 8 and 9 it is clear that

$$A_j^2 \sum_{i=1}^{n} e_{ij}^2 = C_j^2 M_j^2 \sum_{i=1}^{n} e_{ij}^2 = C_j^2 \sum_{i=1}^{n} e_{ip}^2 \quad . \tag{12}$$

In Equation 7 we now make the following substitutions --

For	Substitute	Basis
$A_j V_{ij}$	$C_j Z_{ij}$	Eq. 11
$A_j^2 \sum_{i=1}^{n} e_{ij}^2$	$C_j^2 \sum_{i=1}^{n} e_{ip}^2$	Eq. 12

with the following result:

$$\sum_{i=1}^{n} \left(\sum_{j=1}^{p} C_j Z_{ij} \right)^2 = \left(\sum_{j=1}^{p} C_j^2 \right) \left(\sum_{i=1}^{n} e_{ip}^2 \right) \quad . \tag{13}$$

We rewrite Equation 13 in the following form:

$$\sum_{i=1}^{n} \left[\frac{C_1 Z_{i1} + ... + C_p Z_{ip}}{(C_1^2 + ... + C_p^2)^{1/2}} \right]^2 = \sum_{i=1}^{n} e_{ip}^2 \quad . \tag{14}$$

(It is of interest to note that if we let p = 3, and regard the quantities Z_{i1}, Z_{i2} and Z_{i3} as the rectangular coordinates of a point in three dimensional space, then the expression enclosed in brackets represents the perpendicular distance from the point (Z_{i1}, Z_{i2}, Z_{i3}) to the plane, $C_1 Z_1 + C_2 Z_2 + C_3 Z_3 = 0$).

In the interest of further simplification, we define the constant B_j by

$$B_j \equiv \frac{C_j}{(C_1^2 + ... + C_p^2)^{1/2}} \quad , \tag{15}$$

and write Equation 14 in terms of the new set of constants, as follows:

$$\sum_{i=1}^{n} (B_1 Z_{i1} + ... + B_p Z_{ip})^2 = \sum_{i=1}^{n} e_{ip}^2 \quad . \tag{16}$$

From the definition (Equation 15) of B_j it is clear that

$$B_1^2 + B_2^2 + ... + B_p^2 - 1 = 0 \quad . \tag{17}$$

Values of the coefficients B_1, ..., B_p can be estimated by minimizing the left side of Equation 16, subject to the constraint expressed by Equation 17. From them, estimates of the coefficients A_o, A_1, ..., A_p can be computed as shown in the next section.

B-4 PROCEDURE FOR ESTIMATING THE COEFFICIENTS B_j and A_j

To minimize Equation 16, subject to Equation 17, we employ "Lagrange's method of multipliers"[10], as indicated below.

$$\text{Let } \alpha = \sum_{i=1}^{n} (B_1 Z_{i1} + ... + B_p Z_{ip})^2 \quad , \tag{18}$$

$$\beta = B_1^2 + ... + B_p^2 - 1 = 0, \text{ and} \tag{19}$$

$-\lambda$ = the Lagrange multiplier.

According to the Lagrange technique, α will have an extreme value when the $p + 1$ parameters (λ, B_1, B_2, ..., B_p) have values determined by the following $p + 1$ equations:

$$\begin{aligned}
&\frac{\partial \alpha}{\partial B_1} - \lambda \frac{\partial \beta}{\partial B_1} = 0 \quad , \\
&\frac{\partial \alpha}{\partial B_2} - \lambda \frac{\partial \beta}{\partial B_2} = 0 \quad , \\
&\vdots \\
&\frac{\partial \alpha}{\partial B_p} - \lambda \frac{\partial \beta}{\partial B_p} = 0 \quad .
\end{aligned} \tag{20}$$

By performing the indicated operations on Equations 18 and 19 we form a set of p linear equations corresponding to the p differential equations of Equations 20, and write the result in matrix form as follows:

$$\begin{bmatrix} W_{11} - \lambda & W_{12} & \cdots & W_{1p} \\ W_{21} & W_{22} - \lambda & \cdots & W_{2p} \\ \vdots & & & \\ W_{p1} & W_{p2} & \cdots & W_{pp} - \lambda \end{bmatrix} X \begin{bmatrix} B_1 \\ B_2 \\ \vdots \\ B_p \end{bmatrix} = \begin{bmatrix} 0 \\ 0 \\ \vdots \\ 0 \end{bmatrix} \quad , \tag{21}$$

$$\text{where } W_{jk} = \sum_{i=1}^{n} Z_{ij} Z_{ik} = W_{kj}. \tag{22}$$

Equation 21 has a nontrivial solution if (and only if) the determinant of the p x p matrix in Equation 21 is zero. This determinant can be made zero by choosing an appropriate value of λ. But since there are p values of λ that will make the determinant zero, it is necessary to choose the particular value that will result in minimizing $\sum_{i=1}^{n} e_{ip}^2$. We submit, without proof, that the smallest positive value of λ is the root desired.*

We also assume that the reader is familiar with methods for finding the roots of the determinant of the symmetrical, p x p matrix in Equation 21.[11]

Let $\hat{\lambda}$ be the smallest positive value of λ that will make the determinant zero. We substitute $\hat{\lambda}$ for λ in Equations 21, divide each equation (except the last) by B_p, and form p - 1 linear equations which we express in matrix form below:

$$\begin{bmatrix} W_{11} - \hat{\lambda} & W_{12} & \cdots & W_{1,p-1} \\ W_{21} & W_{22} - \hat{\lambda} & \cdots & W_{2,p-1} \\ \cdot & & & \cdot \\ \cdot & & & \cdot \\ \cdot & & & \cdot \\ \cdot & & & \cdot \\ W_{p-1,1} & W_{p-1,2} & \cdots & W_{p-1,p-1} - \hat{\lambda} \end{bmatrix} \times \begin{bmatrix} B_1/B_p \\ B_2/B_p \\ \cdot \\ \cdot \\ \cdot \\ B_{p-1}/B_p \end{bmatrix} = \begin{bmatrix} -W_{1p} \\ -W_{2p} \\ \cdot \\ \cdot \\ \cdot \\ -W_{p-1,p} \end{bmatrix} \qquad (23)$$

These p-1 equations can be solved for the p - 1 ratios, B_j/B_p (j = 1, ..., p - 1).

Now according to Equation 15,

$$\frac{B_i}{B_p} = \frac{C_i}{C_p} \quad ,$$

and, according to Equation 8,

$$\frac{C_i}{C_p} = \frac{A_i/M_i}{A_p/M_p} \quad ,$$

from which we conclude that

$$\frac{B_i}{B_p} = \frac{A_i/M_i}{A_p/M_p} \quad . \qquad (24)$$

---

* Johnston[10] presents a proof of this statement.

We note from Equation 9 that $M_p = 1$, and (without loss of generality) we also let $A_p = 1$. By substituting 1 for M_p and A_p in Equation 24, we obtain

$$\frac{B_j}{B_p} = \frac{A_j}{M_j} \quad .$$

Thus, we have the following for finding the estimate, $\hat{A}_j$, of A_j:

$$\hat{A}_j = \left(\frac{B_j}{B_p}\right) M_j \quad . \tag{25}$$

Equation 25 is the last step in the solution of the problem. Application of this regression technique presupposes some knowledge of measurement errors for each variable (see, for example, Equation 9). To make the technique somewhat easier to apply, we shall discuss in the next section the concept of the "quality" of a variable, and will present an alternate to Equation 9 for computing the M_j.

B 5. QUALITY OF A VARIABLE

We define the quality, Q_j of the variable, X_j, as the ratio of the variance of X_j to the variance of the errors made in measuring X_j. The equivalent mathematical definition is the dimensionless ratio given below:

$$Q_j \equiv \frac{\sum_{i=1}^{n} (X_{ij} - \bar{X}_j)^2}{\sum_{i=1}^{n} e_{ij}^2} \quad . \tag{26}$$

It may be seen from Equation 26 that if the experiment is so designed that X_j varies widely about its mean, and if the errors made in measuring X_j are small, then the quality of the variable is high. On the other hand, if X_j varies only slightly from its mean and the measurement errors are large, then the quality is low.

From the foregoing it is clear that the quality of a variable depends not only on the precision with which it can be measured, but also upon the design of the experiment.

B-6. Use of the Quality Ratios

From Equations 26 and 9 it can be shown that the constant, M_j, can be defined in terms of the quality ratio, Q_j/Q_p, as follows:

$$M_j \equiv \left[\frac{Q_j}{Q_p} \cdot \frac{\sum_{i=1}^{n} (X_{ip} - \bar{X}_p)^2}{\sum_{i=1}^{n} (X_{ij} - \bar{X}_j)^2} \right]^{1/2} \quad . \qquad (27)$$

The unknown in Equation 27 is the quality ratio, Q_j/Q_p. To compute M_j (a necessary step if the multiple error regression technique is to be used), the investigator must estimate this ratio. This may be difficult, but probably less so than estimating the ratio of the sums of the squared errors as required by Equation 9. Therefore Equation 27, rather than Equation 9, was used for computing M_j in the analysis of Dynaflect data described in this report.

B-7. APPLICATION

This section describes how the equations derived in the preceding sections may be used in estimating the constants in the regression model.

The model is given below:

$$A_o + A_1X_1 + A_2X_2 + ... + A_jX_j + ... + A_{p-1}X_{p-1} + X_p = 0$$

Steps to be followed in estimating the regression coefficients, A_j, are given below in sequence.

1. To each variable, X_j, assign a quality ratio, Q_j/Q_p, where Q_j is defined as follows:

$$Q_j \equiv \frac{\sum_{i=1}^{n} (X_{ij} - \bar{X}_j)^2}{\sum_{i=1}^{n} e_{ij}^2} .$$

2. Compute p values of $\sum_{i=1}^{n} V_{ij}^2$ $(j = 1, ..., p)$ from

$$\sum_{i=1}^{n} V_{ij}^2 = \sum_{i=1}^{n} (X_{ij} - \bar{X}_j)^2 .$$

3. Compute p values of M_j $(j = 1, ..., p)$ from

$$M_j \equiv \left[\frac{Q_j}{Q_p} \cdot \frac{\sum_{i=1}^{n} (X_{ip} - \bar{X}_p)^2}{\sum_{i=1}^{n} (X_{ij} - \bar{X}_j)^2} \right]^{1/2} .$$

4. Compute the p^2 elements of the symmetrical determinant,

$$\begin{vmatrix} W_{11} & W_{12} & \cdots & W_{1p} \\ W_{21} & W_{22} & \cdots & W_{2p} \\ \vdots & & & \\ W_{p1} & W_{p2} & \cdots & W_{pp} \end{vmatrix} ,$$

from the equation

$$W_{jk} = M_j M_k \sum_{i=1}^{n} V_{ij} V_{ik} = W_{kj} \quad .$$

5. Find the least positive value, $\hat{\lambda}$, of λ that satisfies the determinantal equation,

$$\begin{vmatrix} W_{11} - \lambda & W_{12} & \cdots & W_{1p} \\ W_{21} & W_{22} - \lambda & & W_{2p} \\ \vdots & & & \\ W_{p1} & W_{p2} & & W_{pp} - \lambda \end{vmatrix} = 0.$$

(Note that this determinant is formed by subtracting λ from the diagonal elements of the determinant formed in step 4).

6. Solve the following matrix equation for the $p - 1$ ratios, B_j/B_p ($j = 1, \ldots, p - 1$):

$$\begin{bmatrix} W_{11} - \hat{\lambda} & W_{12} & \cdots & W_{1,p-1} \\ W_{21} & W_{22} - \hat{\lambda} & \cdots & W_{2,p-1} \\ \vdots & & & \\ W_{p-1,1} & W_{p-1,2} & \cdots & W_{p-1,p-1} - \hat{\lambda} \end{bmatrix} X \begin{bmatrix} B_1/B_p \\ B_2/B_p \\ \vdots \\ B_{p-1}/B_p \end{bmatrix} = \begin{bmatrix} -W_{1p} \\ -W_{2p} \\ \\ -W_{p-1,p} \end{bmatrix} .$$

7. Find the estimates, $\hat{A}_j$, of the coefficients, A_j, ($j=1, \ldots, p$) from

$$\hat{A}_j = \left(\frac{B_j}{B_p} \right) M_j \quad .$$

8. Find the estimate, $\hat{A}_o$, of the intercept, A_o, from

$$\hat{A}_o = -\sum_{j=1}^{p} \hat{A}_j \bar{X}_j$$

If it is desired to force the regression plane through the origin (A_0 arbitrarily made zero), the procedure is the same as that given above with the following two exceptions:

(a) Change step 2 to read as follows:

2. Compute p values of $\sum_{i=1}^{n} V_{ij}^2$ $(j=1, \ldots, p)$ from

$$\sum_{i=1}^{n} V_{ij}^2 = \sum_{i=1}^{n} X_{ij}^2$$

(b) Eliminate step 8.

(Note that the value of M_j, computed in step 3, is <u>not</u> affected by the change in the definition of V_{ij}, while the matrix element, W_{jk}, computed in step 4, <u>is</u> affected.)

B-8. A NUMERICAL EXAMPLE

To illustrate the effect of variations in the quality ratios, Q_j/Q_p, on the regression coefficients, consider the following numerical example involving only two variables ($p = 2$), and hence only one quality ratio, Q_1/Q_2. The "data" (artifically contrived to emphasize certain features of the multiple error technique), are given in Table B-1.

TABLE B-1

Data for Example

	Measured Values	
	X	X
i	1	2
1	1	5
2	4	2
3	6	7
4	8	12
5	11	9

Using the multiple error method, five analyses of the data were performed, each for a different quality ratio, Q_1/Q_2. The results are given in Table B-2 and are plotted, together with the data, in Figure B-1.

Comparisons with results given by the classical method can be made at extreme values of Q_1/Q_2. For example, if Q_1/Q_2 is made very small, as in Analysis 1 of Table B-2, the coefficients given by the multiple error method approach those computed by the classical procedure when X_1 is regressed on X_2. If Q_1/Q_2 is made very large, as in Analysis 5, the coefficients approach those given by the classical method when X_2 is regressed on X_1.

The result, clearly illustrated in Figure B-1, of making the quality of both variables the same ($Q_1/Q_2 = 1$), is a regression line that follows the visible trend of the data, and bisects the angle between the two lines obtained by the classical method. Also apparent from the figure is the fact that all possible regression lines lie between the extremes given by the classical method.

This two-variable example hopefully will confirm for the reader certain conclusions reached by the writers regarding the multiple error regression technique. These are the following:

(1) The multiple error technique is general in the sense that it includes the classical method as a special case.

(2) If measurement errors exist in more than one of the variables entering into an experiment, estimates of the regression coefficients made by the classical method will be biased. Resort to the multiple error method (if estimates of the quality ratios can be made) may lead to better estimates of the coefficients.

(3) Though the multiple error method (not necessarily under that name) has been discussed in the literature; it has not, to our knowledge, come into general use. It should.

TABLE B-2

Effect of Quality Ratio on Analysis

Model: $A_o + A_1X_1 + X_2 = 0.$

	Multiple Error Method			Classical Method			
Analysis No.	Q_1/Q_2	A_o	A_1	Q_1/Q_2	A_o	A_1	Dependent Variable
1	10^{-6}	1.70000	-1.44500	0	1.70000	-1.44500	X_1
2	0.20	0.87435	-1.31239	--	--	--	--
3	1.00	-1.00000	-1.00000	--	--	--	--
4	5.00	-2.42820	-0.76197	--	--	--	--
5	10^{6}	-2.86207	-0.68966	∞	-2.86207	-0.68966	X_2

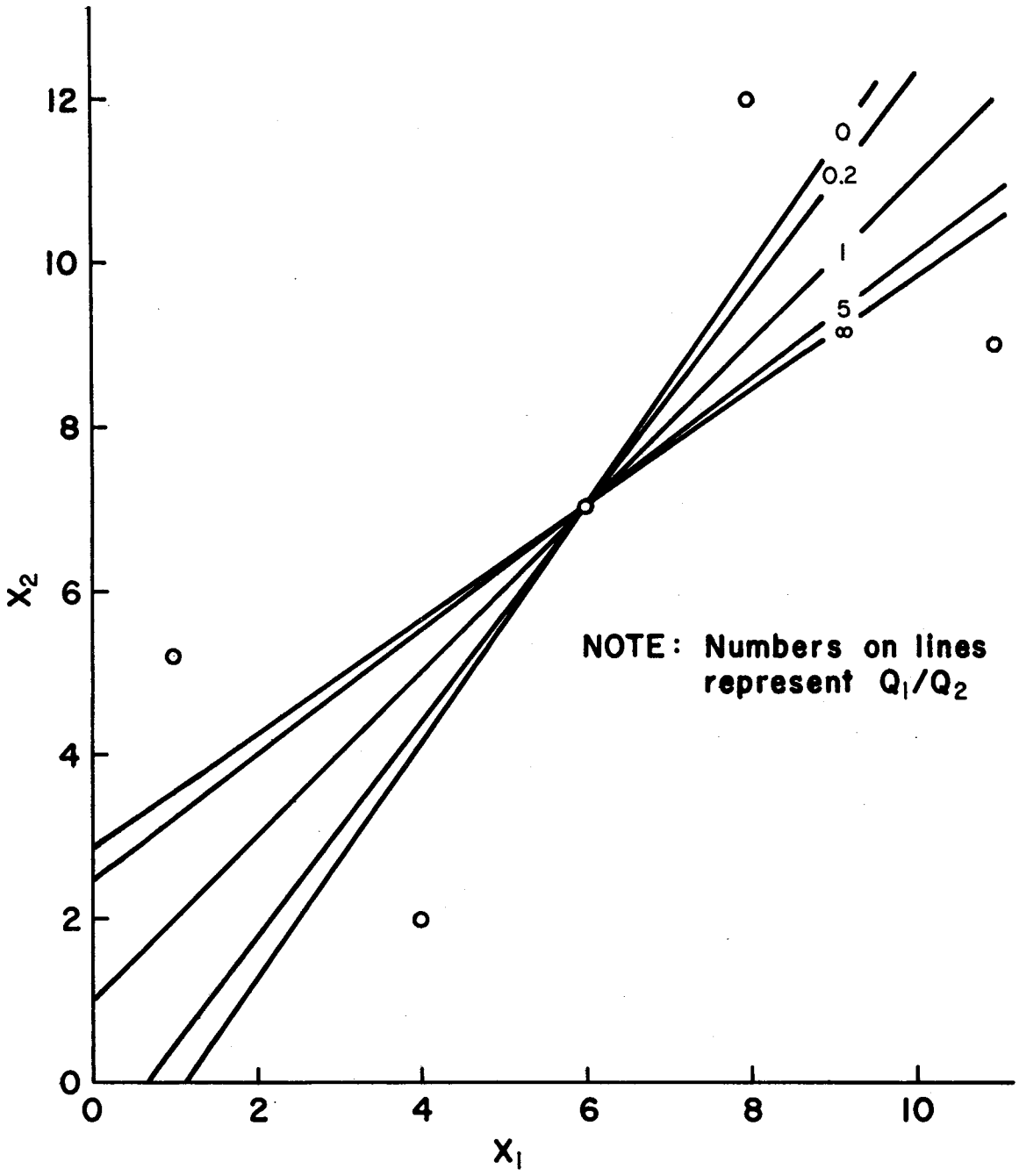

Figure B-1: Effect on the regression line of varying the quality ratio, Q_1/Q_2, in a two-variable analysis. The five circled points represent the data to which the model $A_o + A_1X_1 + X_2 = 0$, was fitted.

B I B L I O G R A P H Y

1. Hartley, H. O., "Smallest Composite Designs for Quadratic Response Surfaces", Biometrics, Vol. 15, No. 4, December, 1959.

2. Michelow, Jr. "Analysis of Stresses and Displacements in an n-Layered Elastic System Under a Load Uniformly Distributed on a Circular Area", California Research Corporation, Richmond, California, September, 1963.

3. Warren, H. and Dieckmann, W. L., "Numerical Computation of Stresses and Strains in a Multiple-Layered Asphalt Pavement System", California Research Corporation, Richmond, California, September, 1963.

4. Terzaghi, Karl, Theoretical Soil Mechanics, John Wiley and Sons, Inc. New York, 1943, pp. 373-376.

5. "Preparation of Soil and Flexible Base Materials for Testing" (Test Method Tex-101-E, Rev.: June 1964) Manual of Testing Procedures, Vol. 1, Texas Highway Department, Materials and Tests Division.

6. Leslie, J. R., "Pulse Techniques Applied to Dynamic Testing," Proceedings, American Society for Testing Materials, Vol. 50, 1950, pp. 1314 to 1323.

7. Birch, F., "The Velocity of Compressional Waves in Rocks to 10 Kilobars, Part I," Journal of Geophysical Research, Vol. 65, No. 4, 1960, pp. 1083-1102.

8. Phelps, J. M. and Cantor, T. R., "Detection of Concrete Deterioration Under Asphalt Overlays by Microseismic Refraction", presented at the 45th annual meeting of the Highway Research Board, Washington, D.C., 1966, in press.

9. Johnston, J., Econometric Methods, McGraw-Hill Book Company, Inc., New York, 1963, pp. 148-176.

10. Sokolnikoff, Ivan S. and Sokolnikoff, Elizabeth S., Higher Mathematics for Engineers and Physicists, McGraw-Hill Book Company, Inc., New York, Second Edition, 1941, pp. 163-167.

11. Crandall, S. H., Engineering Analysis, McGraw-Hill Book Company, Inc., New York, 1956, pp. 118-122.